Generalized Dix equation and analytic treatment of normal-moveout velocity for anisotropic media

Vladimir Grechka*, Ilya Tsvankin* and Jack K. Cohen*

ABSTRACT

Despite the complexity of wave propagation in anisotropic media, reflection moveout on conventional common-midpoint (CMP) spreads is usually well described by the normal-moveout (NMO) velocity defined in the zero-offset limit. In their recent work, Grechka and Tsvankin showed that the azimuthal variation of NMO velocity around a fixed CMP location generally has an *elliptical* form (i.e., plotting the NMO velocity in each azimuthal direction produces an ellipse) and is determined by the spatial derivatives of the slowness vector evaluated at the CMP location. This formalism is used here to develop exact solutions for normal-moveout velocity in anisotropic media of arbitrary symmetry.

For the model of a single homogeneous layer above a dipping reflector, we obtain an *explicit* NMO expression valid for all pure modes and any orientation of the CMP line with respect to the reflector strike. The contribution of anisotropy to normal-moveout velocity is contained in the slowness components of the zero-offset ray (along with the derivatives of the vertical slowness with respect to the horizontal slownesses) – quantities that can be found in a straightforward way from the Christoffel equation. If the medium above a dipping reflector is horizontally stratified, the effective NMO velocity is determined through a Dix-type average of the matrices responsible for the

---

*Center for Wave Phenomena, Colorado School of Mines, Golden, CO 80401-1887

Paper presented at the 59th EAGE Conference, Geneva, 1997.

"interval" NMO *ellipses* in the individual layers. This generalized Dix equation provides an analytic basis for moveout inversion in vertically inhomogeneous, arbitrarily anisotropic media. For models with a throughgoing vertical symmetry plane (i.e., if the dip plane of the reflector coincides with a symmetry plane of the overburden), the semi-axes of the NMO ellipse are found by the more conventional rms averaging of the interval NMO *velocities* in the dip and strike directions.

Modeling of normal moveout in general heterogeneous anisotropic media requires *dynamic* ray tracing of only one (zero-offset) ray. Remarkably, the expressions for geometrical spreading along the zero-offset ray contain all the components necessary to build the NMO ellipse. This method is orders of magnitude faster than multi-azimuth, multi-offset ray tracing and, therefore, can be efficiently used in traveltime inversion and in devising fast dip-moveout (DMO) processing algorithms for anisotropic media. This technique becomes especially efficient if the model consists of homogeneous layers or blocks separated by smooth interfaces.

The high accuracy of our NMO expressions is illustrated by comparison with ray-traced reflection traveltimes in piecewise-homogeneous, azimuthally anisotropic models. We also apply the generalized Dix equation to field data collected over a fractured reservoir and show that P-wave moveout can be used to find the depth-dependent fracture orientation and evaluate the magnitude of azimuthal anisotropy.

INTRODUCTION

Reflection moveout in inhomogeneous anisotropic media is usually calculated by multi-offset and multi-azimuth ray tracing (e.g., Gajewski and Pšenčík 1987). While the existing anisotropic ray-tracing codes are sufficiently fast for forward modeling, their application in moveout inversion requires repeated generation of azimuth-dependent traveltimes around many common-midpoint (CMP) locations, which makes the inversion procedure extremely time-consuming. Moveout model-

ing, however, can be simplified by taking advantage of the limited range of offsets in conventional acquisition design. For spreadlength-to-depth ratios close to unity, CMP traveltimes in media with moderate structural complexity are well described by the normal-moveout (NMO) velocity defined in the zero-spread limit (Tsvankin and Thomsen 1994; Grechka and Tsvankin 1998). Even if the data exhibit nonhyperbolic moveout, NMO velocity is still responsible for the most stable, small-offset portion of the moveout curve.

Existing methods for computing normal-moveout velocity in inhomogeneous media are designed for isotropic models (e.g., Shah 1973; Hubral and Krey 1980). Angular velocity variations make both analytic and computational aspects of NMO-velocity modeling much more complicated. Here, we present a treatment of NMO velocity in inhomogeneous anisotropic media that provides an analytic basis for moveout inversion, leads to a significant increase in the efficiency of traveltime modeling methods, and helps to develop insight into the influence of the anisotropic parameters on reflection traveltimes.

Explicit expressions for normal-moveout velocity are well known for the relatively simple transversely isotropic model with a vertical symmetry axis (VTI media) (e.g., Thomsen 1986). Tsvankin (1995) presented an exact NMO equation for dipping reflectors valid in vertical symmetry planes of any homogeneous anisotropic medium that has such a plane. Alkhalifah and Tsvankin (1995) extended this result by developing a Dix-type equation for vertically *inhomogeneous* anisotropic media above a dipping reflector. They also showed that the NMO-velocity function in VTI media depends on just two parameters – the zero-dip NMO velocity $V_{\rm nmo}(0)$ and the "anellipticity" coefficient η. Still, their formalism is limited to 2-D wave propagation in the dip plane of the reflector, which should also coincide with a symmetry plane of the overburden.

This work is based on a general 3-D treatment of normal moveout developed by Grechka and Tsvankin (1998), who proved that the NMO velocity for pure (non-

converted) modes varies with azimuth as an *ellipse*, even if the medium is arbitrarily anisotropic and inhomogeneous. This conclusion breaks down only for subsurface models in which common-midpoint reflection traveltime cannot be described by a series expansion or does not increase with offset. The orientation of the NMO ellipse and the values of its semi-axes can be expressed through the spatial derivatives of the slowness vector, which are determined by both the direction of the reflector normal and the medium properties above the reflector.

Grechka and Tsvankin (1998) also presented explicit equations for the NMO velocity for two special cases: a horizontal orthorhombic layer and a dipping reflector beneath a VTI medium. A detailed analysis of the NMO ellipse for transversely isotropic media with a horizontal symmetry axis (HTI media) is given in Tsvankin (1997a), who also discusses the inversion of conventional-spread reflection moveout for the parameters of HTI media. Sayers and Ebrom (1997) obtained the elliptical dependence of NMO velocity for the model of a homogeneous anisotropic layer with a horizontal symmetry plane using an approximation for long-spread moveout based on group-velocity expansion in spherical harmonics.

Application of the elliptical NMO equation of Grechka and Tsvankin (1998) in modeling and inversion for arbitrarily anisotropic models requires evaluation of the spatial derivatives of the slowness vector in terms of the model parameters. Here, we accomplish this task for a series of anisotropic models with increasing structural complexity. We start by deriving an explicit expression for azimuth-dependent NMO velocity from a dipping reflector overlaid by a homogeneous anisotropic layer. Then we obtain a generalized Dix equation for NMO velocity in a model composed of a stack of homogeneous, arbitrarily-anisotropic layers with horizontal interfaces above a dipping reflector. While this equation has a form similar to the conventional Dix formula, it is based on the averaging of the *matrices* that define interval NMO *ellipses*. For general inhomogeneous media, we develop an efficient methodology to compute the normal-moveout velocity using the dynamic ray-tracing of only *one* (zero-offset) ray. We show

that the derivatives needed to find the geometrical spreading (e.g., Červeny, Molotkov and Pšenčík 1977; Kendall and Thomson 1989) provide sufficient information to build the NMO ellipse and, therefore, model reflection moveout without tracing a large family of rays. Finally, we compare the hyperbolic moveout equation parameterized by the exact NMO velocity with ray-traced reflection traveltimes and present a field-data application of the generalized Dix differentiation.

EQUATION OF THE NMO ELLIPSE

Suppose the traveltimes of a certain reflected wave (usually called "reflection moveout") have been recorded on a number of common-midpoint (CMP) gathers with different azimuthal orientation but the same midpoint location (Figure 1). If the medium is anisotropic and inhomogeneous, the dependence of large-offset reflection traveltimes on the azimuth α of the CMP line may become rather complicated. For conventional spreadlengths close to the distance between the CMP and the reflector, however, moveout in CMP geometry is usually well-approximated by a hyperbolic equation,

$$t^2(\alpha) \approx t_0^2 + \frac{X^2}{V_{\rm nmo}^2(\alpha)}\,. \tag{1}$$

Here t_0 is the zero-offset reflection time, X is the source-receiver offset, and $V_{\rm nmo}(\alpha)$ is the normal-moveout velocity defined as

$$V_{\rm nmo}^2(\alpha) = \lim_{X\to 0} \frac{d[X^2]}{d[t^2(\alpha)]}\,. \tag{2}$$

According to definition (2), NMO velocity determines the inital slope of the $t^2 - X^2$ curve at zero offset. For any realistic subsurface model, the function $t^2(X^2)$ deviates from a straight line due to the influence of heterogeneity and/or anisotropy, but equation (1) usually remains sufficiently accurate for conventional moderate offsets limited by the distance between the CMP and reflector (Tsvankin and Thomsen 1994; Grechka and Tsvankin 1998).

The analysis below is based on the general result of Grechka and Tsvankin (1998), who showed that NMO velocity is described by the following simple quadratic form:

$$V_{\rm nmo}^{-2}(\alpha) = W_{11}\cos^2\alpha + 2\,W_{12}\sin\alpha\cos\alpha + W_{22}\sin^2\alpha\,, \tag{3}$$

where $\mathbf{W}$ is a symmetric matrix,

$$W_{ij} = \tau_0\,\frac{\partial^2\tau}{\partial x_i \partial x_j}\bigg|_{\mathbf{x}_{\rm CMP}} = \tau_0\,\frac{\partial p_i}{\partial x_j}\bigg|_{\mathbf{x}_{\rm CMP}}\,, \qquad (i,j=1,2)\,. \tag{4}$$

Here, $\tau(x_1,\,x_2)$ is the *one-way* traveltime from the zero-offset reflection point to the location $\mathbf{x}\,\{x_1,\,x_2\}$ at the surface, τ_0 is the one-way zero-offset traveltime, p_i are the components of the slowness vector corresponding to the ray emerging at the point $\mathbf{x}$, and $\mathbf{x}_{\rm CMP}$ is the CMP location. In Figure 1, the common-midpoint coincides with the origin of the coordinate system; however, shifting the origin to any other location does not change the derivatives in equation (4). The one-way traveltimes appear in equation (4) because reflection-point dispersal has no influence on the NMO velocity of pure modes, and (for the small source-receiver offsets appropriate for estimation of $V_{\rm nmo}$) rays can be assumed to propagate through the reflection point of the zero-offset ray (Hubral and Krey 1980; Tsvankin 1995).

It is convenient to use the eigenvectors of the matrix $\mathbf{W}$ as auxiliary horizontal axes and rotate the NMO equation (3) by the angle β (see Appendix A),

$$\beta = \tan^{-1}\left[\frac{W_{22}-W_{11}+\sqrt{(W_{22}-W_{11})^2+4W_{12}^2}}{2W_{12}}\right]\,. \tag{5}$$

This rotation transforms equation (3) into

$$V_{\rm nmo}^{-2}(\alpha) = \lambda_1\cos^2(\alpha-\beta) + \lambda_2\sin^2(\alpha-\beta)\,, \tag{6}$$

where $\lambda_{1,2}$ are the eigenvalues of the matrix $\mathbf{W}$. Grechka and Tsvankin (1998) conclude that for positive λ_1 and λ_2 the NMO velocity (3) plotted in each azimuthal direction defines a centered *ellipse*. A negative eigenvalue implies a negative $V_{\rm nmo}^2$ in certain azimuthal directions and, consequently, a decrease in the CMP traveltime

with offset. Although such reverse moveout can exist in some cases (e.g., for turning waves, as described by Hale et al. 1992), typically both λ_1 and λ_2 are positive, and the azimuthal dependence of NMO velocity is indeed elliptical. Note that this conclusion is valid for arbitrarily inhomogeneous anisotropic media provided the traveltime field is sufficiently smooth to be adequately approximated by a Taylor series expansion.

HOMOGENEOUS ARBITRARILY ANISOTROPIC LAYER

General case

To obtain normal-moveout velocity for any given model from equations (3) and (4), we need to evaluate the spatial derivatives of the slowness vector at the CMP location. As demonstrated in Appendix B, for the model of a single homogeneous layer this can be done by representing the horizontal ray displacement through group velocity and using the relation between the group-velocity and slowness vectors. As a result, we find the following explicit expressions for the matrix $\mathbf{W}$ and azimuth-dependent NMO velocity [equations (B-8) and (B-9)]:

$$\mathbf{W} = \frac{p_1 q_{,1} + p_2 q_{,2} - q}{q_{,11} q_{,22} - q_{,12}^2} \begin{pmatrix} q_{,22} & -q_{,12} \\ -q_{,12} & q_{,11} \end{pmatrix} , \tag{7}$$

$$\begin{aligned} V_{\rm nmo}^{-2}(\alpha) &\equiv V_{\rm nmo}^{-2}(\alpha, p_1, p_2) \\ &= \frac{p_1 q_{,1} + p_2 q_{,2} - q}{q_{,11} q_{,22} - q_{,12}^2} \left[q_{,22} \cos^2\alpha - 2 q_{,12} \sin\alpha \cos\alpha + q_{,11} \sin^2\alpha \right] , \end{aligned} \tag{8}$$

where $q \equiv q(p_1, p_2) \equiv p_3$ denotes the vertical slowness component, $q_{,i} \equiv \partial q / \partial p_i$, and $q_{,ij} \equiv \partial^2 q / \partial p_i \partial p_j$; the horizontal components of the slowness vector (p_1 and p_2) and the derivatives in equation (8) are evaluated for the zero-offset ray.

Equation (8) is valid for pure modes reflected from horizontal or dipping interfaces in media with arbitrary symmetry and any strength of the anisotropy (i.e., for any magnitude of the anisotropic parameters). The normal-moveout velocity is fully determined by the azimuth α of the CMP line and the slowness vector of the zero-offset

ray. The slowness components p_1, p_2 and q can be found by solving the Christoffel equation for the slowness (phase) direction normal to the reflector. (The slowness vector of the zero-offset ray is normal to the reflecting interface at the reflection point.) Since this equation is cubic with respect to the squared phase velocity, it yields an explicit expression for the slowness vector.

The derivatives of the vertical slowness q can be found directly from the Christoffel equation as well. The slowness components satisfy the equation $F(q, p_1, p_2) = 0$, where F is (in general) a sixth-order polynomial with respect to q. Note that for anisotropic models with a horizontal symmetry plane (e.g., the medium can be transversely isotropic, orthorhombic or even monoclinic), F becomes a *cubic* polynomial with respect to q^2. Hence, the derivatives $q_{,i}$ and $q_{,ij}$ can be obtained as

$$q_{,i} = -\frac{F_{p_i}}{F_q}$$

and

$$q_{,ij} = -\frac{F_{p_ip_j} + F_{p_iq}q_{,j} + F_{p_jq}q_{,i} + F_{qq}q_{,i}q_{,j}}{F_q}\,, \tag{9}$$

where $F_{p_i} \equiv \partial F/\partial p_i$, $F_q \equiv \partial F/\partial q$, $F_{p_ip_j} \equiv \partial^2 F/\partial p_i \partial p_j$, $F_{p_iq} \equiv \partial^2 F/\partial p_i \partial q$, and $F_{qq} \equiv \partial^2 F/\partial q^2$. Therefore, all terms in equation (8) can be obtained *explicitly* from the Christoffel equation.

Equation (8) can also be used to develop weak-anisotropy approximations for NMO velocity by linearizing q and its derivatives in dimensionless anisotropic parameters or in perturbations in the stiffness coefficients. These analytic approximations provide valuable insight into the influence of the anisotropic parameters on normal moveout (e.g., Tsvankin 1995; Cohen 1998). There is hardly any need, however, to substitute weak-anisotropy approximations for the exact equations in numerical modeling.

Thus, equation (8) gives a simple and numerically efficient recipe to obtain azimuth-dependent reflection moveout in an arbitrarily anisotropic layer. The example in Figure 2, generated for an orthorhombic layer above a dipping reflector,

illustrates the high accuracy of the hyperbolic moveout equation parameterized by the analytic NMO velocity (8) in describing conventional-spread reflection traveltimes. Despite the presence of anisotropy-induced nonhyperbolic moveout, the P-wave NMO velocity is close to the moveout (stacking) velocity calculated from the exact traveltimes on six CMP lines with different orientation. The maximum difference between $V_{\rm nmo}$ (solid line) and the finite-spread moveout velocity (dots) is just 1.4%, which is even less than the corresponding value (2.7%) for the same model, but with a *horizontal* reflector (see Grechka and Tsvankin 1998). Therefore, the magnitude of nonhyperbolic moveout for this model decreases with reflector dip; the same observation was made by Tsvankin (1995) for vertical transverse isotropy. Note that although the azimuth of the dip plane of the reflector is equal to 30°, the semi-major axis of the $V_{\rm nmo}(\alpha)$ ellipse has an azimuth of 24.3° due to the influence of the azimuthal anisotropy above the reflector.

Special cases

Model with a vertical symmetry plane.—Next, let us consider a special case – a model in which the dip plane of the reflector coincides with a vertical symmetry plane of the layer. The medium can be, for instance, transversely isotropic, orthorhombic or monoclinic. The mirror symmetry with respect to the dip plane implies that one of the axes of the NMO ellipse points in the dip direction. Below, we provide a formal proof of this fact, as well as concise expressions for the azimuth-dependent NMO velocity in this model.

It is convenient to align the x_1-axis with the azimuth of the dip plane, while the x_2-axis will point in the strike direction. Evidently, the zero-offset ray should lie in the vertical symmetry plane $x_2 = 0$, and its slowness component p_2 goes to zero. As another consequence of the mirror symmetry with respect to the dip plane, $\partial p_2/\partial x_1 = 0$ (i.e, rays corresponding to $x_2 = 0$ stay in the dip plane and cannot have

a non-zero p_2), so the cross-term $q_{,12}$ in equation (8) vanishes, and the NMO velocity simplifies to

$$V_{\rm nmo}^{-2}(\alpha, p_1) = \frac{p_1 q_{,1} - q}{q_{,11} q_{,22}} \left[q_{,22} \cos^2\alpha + q_{,11} \sin^2\alpha \right] . \tag{10}$$

Equation (10) describes an ellipse with the semi-axes in the dip ($\alpha = 0$) and strike ($\alpha = \pi/2$) directions:

$$V_{\rm nmo}^2(\alpha = 0, p_1) = \frac{q_{,11}}{p_1 q_{,1} - q} , \tag{11}$$

$$V_{\rm nmo}^2(\alpha = \frac{\pi}{2}, p_1) = \frac{q_{,22}}{p_1 q_{,1} - q} . \tag{12}$$

The dip-line NMO velocity (11) was originally obtained via the in-plane phase velocity V by Tsvankin (1995):

$$V_{\rm nmo}(0, \phi) = \frac{V(\phi)}{\cos\phi} \frac{\sqrt{1 + \frac{1}{V(\phi)} \frac{d^2 V}{d\theta^2}|_{\theta=\phi}}}{1 - \frac{\tan\phi}{V(\phi)} \frac{dV}{d\theta}|_{\theta=\phi}} , \tag{13}$$

where θ is the phase angle with vertical in the dip plane, and ϕ is the reflector dip. In the form (11) $V_{\rm nmo}^2(0, p_1)$ was first given by Cohen (1998). Equation (12) provides a similar representation for the NMO velocity in the strike direction.

Equations (11) and (12) are always valid for transversely isotropic media with a vertical symmetry axis because of the mirror symmetry with respect to *any* vertical plane in this model. The vertical slowness in VTI media can be represented as $q(p_1, p_2) \equiv q\left(\sqrt{p_1^2 + p_2^2}\right)$ and, for $p_2 = 0$, $q_{,22} = q_{,1}/p_1$. Then equation (12) for the strike-line NMO velocity reduces to the expression obtained previously by Grechka and Tsvankin (1998),

$$V_{\rm nmo}^2(\alpha = \frac{\pi}{2}, p_1) = \frac{q_{,1}}{p_1 (p_1 q_{,1} - q)} . \tag{14}$$

Grechka and Tsvankin (1998) also gave an equivalent form of equation (14) in terms of the phase-velocity function and the weak-anisotropy approximation for $V_{\rm nmo}^2(\alpha = \frac{\pi}{2}, p_1)$. Due to the axial symmetry of the VTI model, both the dip-line

[equation (11)] and strike-line [equation (14)] NMO velocities depend on the derivatives of q with respect to the single horizontal (in-plane) slowness component (p_1). The cubic equation for $q^2(p_1)$ in VTI media is particularly easy to solve because it splits into a quadratic equation for $P-SV$ waves and a linear equation for the SH-wave.

Finally, in isotropic media the vertical slowness can be directly expressed through the reflector dip ϕ:

$$q = \sqrt{V^{-2} - p_1^2} = \frac{\cos\phi}{V}\,,$$

and equations (13) and (14) yield the well-known relationships presented by Levin (1971):

$$V_{\rm nmo}(\alpha = 0) = \frac{V}{\cos\phi}\,, \tag{15}$$

$$V_{\rm nmo}(\alpha = \frac{\pi}{2}) = V\,. \tag{16}$$

Horizontal reflector.—For a horizontal reflector ($p_1 = p_2 = 0$), equation (8) reduces to

$$V_{\rm nmo}^{-2}(\alpha, 0, 0) = -\frac{q}{q_{,11}q_{,22} - q_{,12}^2}\,\left[q_{,22}\cos^2\alpha - 2q_{,12}\sin\alpha\cos\alpha + q_{,11}\sin^2\alpha\right]\,, \tag{17}$$

where q and $q_{,ij}$ should be evaluated at the vertical slowness direction.

Further simplification can be achieved for a medium with a vertical symmetry plane. Aligning the x_1-axis with the symmetry-plane direction and substituting $p_1 = 0$ into equation (10) [or $q_{,12} = 0$ into equation (17)] yields

$$V_{\rm nmo}^{-2}(\alpha) = -\frac{q}{q_{,11}q_{,22}}\,\left[q_{,22}\cos^2\alpha + q_{,11}\sin^2\alpha\right]\,. \tag{18}$$

As shown by Grechka and Tsvankin (1998), for an orthorhombic layer (that has two mutually orthogonal symmetry planes) P-wave NMO velocity from equation (18) becomes a simple function of the vertical P-wave velocity V_{P0} and the anisotropic coefficients $\delta^{(1)}$ and $\delta^{(2)}$ defined by Tsvankin (1997b):

$$V^2_{\rm nmo}(\alpha) = V^2_{P0}\,\frac{(1+2\delta^{(1)})\,(1+2\delta^{(2)})}{1+2\delta^{(2)}\sin^2\alpha+2\delta^{(1)}\cos^2\alpha}\,. \qquad (19)$$

Note that the linearized δ coefficients introduced by Mensch and Rasolofosaon (1997) and Gajewski and Pšenčík (1996) within the framework of the weak-anisotropy approximation are not appropriate for the exact equation (19). Normal-moveout velocities for vertical and horizontal transverse isotropy can be easily found as special cases of equation (19) (Grechka and Tsvankin 1998). Equation (18) can also be used to derive similar expressions for the split shear waves in orthorhombic media.

HORIZONTALLY LAYERED MEDIUM ABOVE A DIPPING REFLECTOR

Generalized Dix equation

Here, we show that the NMO ellipse for vertically inhomogeneous arbitrarily anisotropic media above a dipping reflector (Figure 3) can be obtained by Dix-type averaging of the matrices $\mathbf{W}$ responsible for the interval NMO ellipses. In our derivation we essentially follow the approach employed by Alkhalifah and Tsvankin (1995) to obtain a "2-D" Dix-type NMO equation for rays confined to the incidence (vertical) plane that cointains the CMP line. Their equation is valid only in the dip plane of the reflector, which should also coincide with a symmetry plane of the medium. In contrast, we make no assumptions about the mutual orientation of the CMP line and reflector strike, and take full account of the out-of-plane phenomena associated with both model geometry and depth-varying anisotropy.

To construct the effective NMO ellipse, we need to obtain the matrix $\mathbf{W}$ defined in equation (4):

$$W_{ij}(L) = \tau(L)\frac{\partial p_i}{\partial x_j(L)}\,, \qquad (i,j=1,2)\,, \qquad (20)$$

where $\tau(L)$ is the total zero-offset traveltime and $x_i(L)$ is the horizontal ray displacement between the zero-offset reflection point located at the L-th (generally dipping)

interface and the surface (Figure 3). Due to the continuity of the ray, both $\tau(L)$ and $x_i(L)$ are equal to the sum of the respective interval values:

$$\tau(L) = \sum_{\ell=1}^{L} \tau_\ell \,, \tag{21}$$

$$x_i(L) = \sum_{\ell=1}^{L} x_{i,\ell} \,, \qquad (i = 1, 2). \tag{22}$$

(Note that here and below in the section on layered media, the comma in the subscripts separates the layer index and *does not* denote differentiation.)

It is convenient to introduce an auxiliary matrix

$$Y_{ij}(L) \equiv \frac{\partial x_i(L)}{\partial p_j} \,, \qquad (i, j = 1, 2) \tag{23}$$

with derivatives evaluated for the ray parameters p_1 and p_2 of the zero-offset ray. Then

$$\mathbf{W} \equiv \mathbf{W}(L) = \tau(L)\, \mathbf{Y}^{-1}(L) \,. \tag{24}$$

In a model composed of homogeneous layers with horizontal interfaces above the reflector, the horizontal components p_1 and p_2 of the slowness vector remain constant along any given ray between the reflection point and the surface. Therefore, substituting equation (22) into equation (23), we find

$$Y_{ij}(L) \equiv \frac{\partial x_i(L)}{\partial p_j} = \sum_{\ell=1}^{L} \frac{\partial x_{i,\ell}}{\partial p_j} \equiv \sum_{\ell=1}^{L} Y_{ij,\ell} \,. \tag{25}$$

Equation (25) explains the reason for introducing the effective matrix $\mathbf{Y}(L)$: unlike the matrix $\mathbf{W}$, it can be decomposed into the sum of the matrices $\mathbf{Y}_\ell$ for the individual layers. Since all intermediate boundaries are horizontal, the ray displacements $x_{i,\ell}$ in any layer coincide with the values that should be used in computing the matrix $\mathbf{W}$ and the interval NMO velocity for this particular layer. Hence, we can apply equation (24) to layer ℓ:

$$\mathbf{W}_\ell = \tau_\ell\, \mathbf{Y}_\ell^{-1} \tag{26}$$

and, therefore,

$$\mathbf{Y}_\ell = \tau_\ell \, \mathbf{W}_\ell^{-1} \, . \tag{27}$$

Substituting equations (27) and (25) into equation (24) leads to the final result:

$$\mathbf{W}^{-1}(L) = \frac{1}{\tau(L)} \sum_{\ell=1}^{L} \tau_\ell \, \mathbf{W}_\ell^{-1} \, . \tag{28}$$

Interval matrices $\mathbf{W}_\ell$ in terms of the components of the slowness vector are given by equation (7), while the traveltimes τ_ℓ should be obtained from the kinematic ray tracing (i.e., by computing group velocity) of the zero-offset ray. Note that, since the eigenvalues of the matrices $\mathbf{W}_\ell$ and $\mathbf{W}(L)$ usually are positive (under the assumptions discussed in Grechka and Tsvankin 1998), these matrices are nonsingular and, therefore, can be inverted.

Equation (28) performs Dix-type averaging of the interval matrices $\mathbf{W}_\ell$ to obtain the effective matrix $\mathbf{W}(L)$ and the effective normal-moveout velocity $V_{\rm nmo}(\alpha, L)$. It should be emphasized that the interval NMO velocities $V_{{\rm nmo},\ell}(\alpha)$ (or the interval matrices $\mathbf{W}_\ell$) in equation (28) are computed for the horizontal components of the slowness vector of the zero-offset ray. Note that the slowness vector of the zero-offset ray is normal to the reflector at the reflection point. This means that the interval matrices $\mathbf{W}_\ell$ in equation (28) correspond to the generally *non-existent* reflectors that are orthogonal to the slowness vector of the zero-offset ray in each layer.

Rewriting equation (28) in the "Dix differentiation" form gives

$$\mathbf{W}_\ell^{-1} = \frac{\tau(\ell)\mathbf{W}^{-1}(\ell) - \tau(\ell-1)\mathbf{W}^{-1}(\ell-1)}{\tau(\ell) - \tau(\ell-1)} \, . \tag{29}$$

Equations (28) and (29) generalize the Dix (1955) formula for horizontally-layered arbitrarily anisotropic media above a dipping reflector. Formally, this extention looks relatively straighforward: the squared NMO velocities in the Dix formula are simply replaced by the inverse matrices $\mathbf{W}^{-1}$. Also, the generalized Dix differentiation is subject to the same limitation as its conventional counterpart: the thickness of the

layer of interest (in vertical time) should not be too much smaller than the layer's depth.

In contrast to the conventional Dix equation, however, the effective matrix $\mathbf{W}^{-1}(\ell-1)$ in equation (29) *cannot* be obtained from seismic data directly since the corresponding reflector usually does not exist in the subsurface. Therefore, layer-stripping by means of equation (29) involves recalculating each interval matrix $\mathbf{W}_\ell$ from one value of the slowness vector (corresponding to a certain real reflector in a given layer) to another – that of the zero-offset ray. This procedure was discussed for the 2-D case by Alkhakifah and Tsvankin (1995) and further developed for P-waves in VTI media by Alkhalifah (1997); the latter paper also contains an application of this algorithm to field data.

Only in the simplest special case of a *horizontal* reflector, does the slowness vector of the zero-offset ray keep its direction (stays vertical) all the way to the surface, and the interval matrices $\mathbf{W}_\ell$ correspond to the NMO velocities from horizontal interfaces that can be measured from reflection data. Note that although such a model is horizontally-homogeneous, the zero-offset *ray* is not necessarily vertical (if the medium does not have a horizontal symmetry plane), and the zero-offset reflection point may be shifted in the horizontal direction from the CMP location.

Model with a vertical symmetry plane

Next, we consider the same special case as for the single-layer model – a medium in which all layers have a common vertical symmetry plane that coincides with the dip plane of the reflector (e.g., the symmetry is VTI). For such a model the matrices $\mathbf{W}_\ell$ in the individual layers are diagonal (see the previous section), and

$$W_{12,\ell} = 0\,. \tag{30}$$

Consequently, the off-diagonal elements of the matrix $\mathbf{W}(L)$ [equation (28)] vanish as well:

$$W_{12}(L) = 0\,. \tag{31}$$

If the matrix $\mathbf{W}$ is diagonal, its two components directly determine the semi-axes of the NMO ellipse [see equation (3) and Appendix A]:

$$W_{kk,\ell} = [V^{(k)}_{\mathrm{nmo},\ell}]^{-2} \tag{32}$$

and

$$W_{kk}(L) = [V^{(k)}_{\mathrm{nmo}}(L)]^{-2}\,, \qquad (k = 1, 2)\,, \tag{33}$$

where $[V^{(1)}_{\mathrm{nmo}} \equiv V_{\mathrm{nmo}}(\alpha = 0)]$ and $[V^{(2)}_{\mathrm{nmo}} \equiv V_{\mathrm{nmo}}(\alpha = \pi/2)]$ are the NMO velocities measured in the dip and strike directions, respectively.

Substitution of equations (30) – (33) into equations (28) and (29) yields more conventional Dix-type averaging and differentiation formulas for the dip- and strike-components of the normal-moveout velocity:

$$[V^{(k)}_{\mathrm{nmo}}(L)]^2 = \frac{1}{\tau(L)} \sum_{\ell=1}^{L} \tau_\ell\, [V^{(k)}_{\mathrm{nmo},\ell}]^2 \tag{34}$$

and

$$[V^{(k)}_{\mathrm{nmo},\ell}]^2 = \frac{\tau(\ell)[V^{(k)}_{\mathrm{nmo}}(\ell)]^2 - \tau(\ell-1)[V^{(k)}_{\mathrm{nmo}}(\ell-1)]^2}{\tau(\ell) - \tau(\ell-1)}\,, \qquad (k = 1, 2)\,. \tag{35}$$

Equations (34) and (35) for the *dip* component ($k = 1$) of the NMO velocity were derived by Alkhalifah and Tsvankin (1995) who considered 2-D wave propagation in the dip plane of the reflector. Our derivation shows that the same Dix-type equations can be applied to the *strike*-component ($k = 2$) of the NMO velocity, which determines the second semi-axis of the NMO ellipse. Despite the close resemblance of expressions (34) and (35) to the conventional Dix equation, the interval NMO velocities in equations (34) and (35), as in the more general Dix equation discussed above, correspond to the *non-existent* reflectors normal to the slowness vector of the zero-offset ray in each layer.

Accuracy of the rms averaging of NMO velocities

Although the generalized Dix equation (28) operates with the *matrices* $\mathbf{W}_\ell^{-1}$, we proved that Dix-type averaging can be applied to the dip- and strike-components of the *normal-moveout velocity* in a model that has a common (throughgoing) vertical symmetry plane aligned with the dip plane of the reflector. It is also clear from the results of the previous section that the rms averaging of the interval NMO velocities is valid in any azimuthal direction, if all interval NMO ellipses degenerate into circles. Hence, the error of this more conventional averaging procedure depends on the elongation of the interval ellipses, a quantity controlled by both azimuthal anisotropy and reflector dip. In Appendix C we show that this error increases rather slowly as the interval ellipses pull away from a circle because the rms averaging of the interval velocities [equation (C-3)] provides a *linear* approximation to the exact NMO velocity, if both are expanded in the "elongation" coefficient.

To quantify this conclusion, we consider two numerical examples. Figure 4 shows the azimuth-dependent P-wave NMO velocity in an orthorhombic medium consisting of three horizontal layers with strong azimuthal anisotropy. While the exact NMO ellipse (solid line) happens to be close to a circle, the approximate, rms-averaged normal-moveout velocity (dashed line) has an oval nonelliptical shape because the interval NMO ellipses differ significantly from circles. The maximum error of the rms averaging is about 6.3%, which will lead to much higher errors in the interval velocities after application of the Dix differentiation (35). Evidently, for this model it is necessary to use the exact NMO equation, which properly accounts for the influence of azimuthal anisotropy on normal moveout.

For models with moderate azimuthal anisotropy and a horizontal reflector (i.e., with the interval NMO-velocity variation limited by 10-20%), the accuracy of the rms averaging of NMO velocites is much higher. This implies that for such media it is possible to obtain the interval NMO velocity by the conventional Dix differentiation

at a given azimuth. In the special case of horizontally layered HTI media (transverse isotropy with a horizontal axis of symmetry), the same conclusion was made by Al-Dajani and Tsvankin (1996).

It should be emphasized, however, that for *dipping* reflectors the Dix differentiation *cannot* be applied in the standard fashion (even if the rms-averaging equation provides sufficient accuracy) because the interval NMO velocities are still calculated for non-existent reflectors and cannot be found directly from the data. In the presence of anisotropy, interval parameter estimation using dipping events is impossible without a layer-stripping procedure that requires reconstruction of the NMO ellipses in the overburden and, therefore, cannot be carried out for a single azimuth.

On the whole, we would recommend to use the generalized Dix equation for *any* azimuthally anisotropic model, provided the azimuthal coverage of the data is sufficient to obtain the dependence $V_{\rm nmo}(\alpha)$. Since our algorithm operates with the NMO ellipses rather than individual azimuthal moveout measurements, it has the additional advantage of smoothing the azimuthal variation of NMO velocity, which helps to eliminate "outliers" and stabilize the interval parameter estimation. A field-data application of the generalized Dix equation is discussed below.

Another example, in which the interval NMO ellipses differ from circles due to the influence of reflector dip in a purely *isotropic* layered model, is shown in Figure 5. Obviously, in this model the dip plane of the reflector always represents a symmetry plane, and one of the axes of all interval NMO ellipses is parallel to the dip direction. As shown in the previous section, in this case the rms averaging of the interval NMO velocities [equations (34) or (35)] becomes exact for the dip (azimuth $\alpha = 0^\circ$) and strike CMP lines (azimuth $\alpha = 90^\circ$), where the interval NMO values are well known (Levin 1971). Figure 5 corroborates this conclusion: for azimuths $\alpha = 0^\circ$ and $\alpha = 90^\circ$ the rms-averaged NMO velocity $\tilde{V}_{\rm nmo}$ is equal to the exact value $V_{\rm nmo}$. In all other azimuths, equation (C-3) gives only an approximation to the exact NMO velocity. However, Figure 5 indicates that this approximation is quite accurate for small and

moderate reflector dips. The maximum error of equation (C-3), for example, is only 0.22% for reflector dip $\phi = 40^\circ$ and 1.85% for dip $\phi = 60^\circ$. Clearly, the error increases with dip because the interval NMO ellipses become more elongated and diverge more from a circle.

Again, since the reflector is dipping, the interval NMO velocities in Figure 5 are calculated for the nonzero horizontal components of the slowness vector determined by the reflector dip. These interval velocities correspond to non-existent reflectors and need to be recalculated from the NMO velocities of the horizontal events (which is, however, straightforward for isotropic media).

INHOMOGENEOUS ANISOTROPIC MEDIA

The results of Grechka and Tsvankin (1998), briefly reviewed above, show that there is no need to perform a full-scale multi-azimuth ray tracing to compute reflection traveltimes on conventional CMP spreads. It is clear from equation (3) that the NMO ellipse (6) and conventional-spread moveout as a whole are fully defined by only three quantities – W_{11}, W_{12}, and W_{22}. Thus, three well-separated azimuthal measurements of $V_{\rm nmo}(\alpha)$ [which usually can be obtained using hyperbolic semblance analysis based on equation (1)] are sufficient to reconstruct the NMO ellipse and find the NMO velocity for any azimuth α. In practice, the values of $V_{\rm nmo}(\alpha)$ determined on finite CMP spreads may be distorted by the influence of nonhyperbolic moveout. However, reflection moveout (especially that of P-waves) for spreadlengths close to the distance of the CMP from the reflector is typically close to hyperbolic; this has been shown in a number of publications (Tsvankin and Thomsen 1994; Tsvankin 1995; Grechka and Tsvankin 1998) and is further illustrated by numerical examples in this work.

Although calculation of W_{ij} from $V_{\rm nmo}(\alpha)$ obtained in three azimuths is much more efficient than multi-azimuth ray tracing, it still requires a considerable amount of computation and does not take advantage of the explicit expressions for the pa-

rameters of the NMO-velocity ellipse discussed above. It is much more attractive to build the NMO ellipse directly from equations (3) and (4), which requires obtaining the spatial derivatives of the ray parameter $\partial p_i/\partial x_j$ at the CMP location (i.e., for the zero-offset ray). Here, we outline an efficient method of calculating these derivatives based on the dynamic ray-tracing equations for the zero-offset ray.

Let us consider the zero-offset ray in the ray coordinates $(\gamma_1, \gamma_2, \tau)$. The parameter τ has the meaning of the traveltime along the ray, while γ_1 and γ_2 are supposed to uniquely determine the raypath and can be chosen, for instance, as the horizontal components of the slowness vector (p_1 and p_2). Here, we use another option suggested by Kashtan (1982) and Kendall and Thomson (1989), and define γ_1 and γ_2 as the polar and azimuthal angles of the slowness (wave-normal) vector.

The derivatives $\partial p_i/\partial x_j$, needed to calculate $V_{\rm nmo}(\alpha)$, can be formally written as

$$\frac{\partial p_i}{\partial x_j} = \frac{\partial p_i}{\partial \gamma_1}\,\frac{\partial \gamma_1}{\partial x_j} + \frac{\partial p_i}{\partial \gamma_2}\,\frac{\partial \gamma_2}{\partial x_j} + \frac{\partial p_i}{\partial \tau}\,\frac{\partial \tau}{\partial x_j}\,. \tag{36}$$

Using the matrix notation

$$\mathbf{P} = \left[\frac{\partial \mathbf{p}}{\partial \gamma_1}, \frac{\partial \mathbf{p}}{\partial \gamma_2}, \frac{\partial \mathbf{p}}{\partial \tau}\right], \qquad \mathbf{X} = \left[\frac{\partial \mathbf{x}}{\partial \gamma_1}, \frac{\partial \mathbf{x}}{\partial \gamma_2}, \frac{\partial \mathbf{x}}{\partial \tau}\right] \tag{37}$$

and the fact that the inverse matrix $\mathbf{X}^{-1}$ contains the rows

$$\mathbf{X}^{-1} = \begin{bmatrix} \partial\gamma_1/\partial\mathbf{x} \\ \partial\gamma_2/\partial\mathbf{x} \\ \partial\tau/\partial\mathbf{x} \end{bmatrix},$$

we represent equation (36) in the form

$$\frac{\partial p_i}{\partial x_j} = \mathbf{P}\,\mathbf{X}^{-1}\,. \tag{38}$$

Hence, if the matrices (37) have been calculated for the zero-offset ray at the CMP (surface) location, the derivatives $\partial p_i/\partial x_j$, $(i, j = 1, 2)$ can be determined as the upper-left 2×2 submatrix of the 3×3 matrix (38). Note that the values of $\partial p_i/\partial x_j$ used in the NMO-velocity calculation correspond to one-way propagation from the

zero-offset reflection point to the surface (Grechka and Tsvankin, 1998). In other words, both $\mathbf{p}$ and $\mathbf{x}$ should be computed for rays emanating from an imaginary source located at the reflection point of the zero-offset ray.

The third column of the matrices $\mathbf{P}$ and $\mathbf{X}$ [i.e. the derivatives $\partial\mathbf{p}/\partial\tau$ and $\partial\mathbf{x}/\partial\tau$] can be obtained directly from the equations of kinematic ray-tracing. To find the first and second columns [i.e., the derivatives $\partial\mathbf{p}/\partial\gamma_n$ and $\partial\mathbf{x}/\partial\gamma_n$, $(n = 1, 2)$], we need to integrate so-called dynamic ray-tracing equations (e.g., Červeny, Molotkov and Pšenčík 1977; Kendall and Thomson 1989). The derivatives needed to obtain the normal-moveout velocity are exactly the same as those required to compute the geometrical spreading along the zero-offset ray. This result is not entirely surprising because NMO velocity is related to the wavefront curvature (Shah 1973), which, in turn, determines geometrical spreading.

Thus, the azimuth-dependent NMO velocity in inhomogeneous arbitrarily anisotropic media can be computed by integrating the dynamic ray-tracing equations for the one-way zero-offset ray and substituting the results into equations (38), (4) and (3). The zero-offset traveltime τ_0 required in equation (4) can be found using kinematic ray tracing (e.g., Červeny 1972; Kendall and Thomson 1989). Since this approach requires dynamic tracing of only *one* zero-offset ray, it is orders of magnitude less time consuming than is the tracing of hundreds of reflected rays for different azimuths and source-receiver offsets as would otherwise be needed.

In the special case of a medium composed of arbitrarily anisotropic *homogeneous* layers (or blocks) separated by smooth interfaces, the ray trajectory becomes piecewise linear, and the integration of the kinematic ray-tracing equations reduces to summation along straight ray segments. Integration of the dynamic ray-tracing equations becomes relatively straightforward as well, because it only requires the continuation of the derivatives $\partial\mathbf{x}/\partial\gamma_n$ and $\partial\mathbf{p}/\partial\gamma_n$ across homogeneous layers and (smooth) interfaces (Kashtan 1982). For plane interfaces, Kashtan's results become especially simple and include only quantities which are obtained during the kinematic ray-

tracing anyway (e.g., the group velocity and traveltime). Therefore, the additional cost of computing the derivatives $\partial\mathbf{x}/\partial\gamma_n$ and $\partial\mathbf{p}/\partial\gamma_n$ in this case is minimal.

SYNTHETIC EXAMPLES

The accuracy of our single-layer NMO equation has been discussed above (see Figure 2). Here, we carry out synthetic tests to compare the hyperbolic moveout equation parameterized by the exact NMO velocity with ray-traced traveltimes for inhomogeneous anisotropic models.

Figure 7 illustrates the performance of the Dix equation (28) for a model that includes three anisotropic layers with different symmetry above a dipping reflector (Figure 6). We used ray tracing to calculate P-wave reflection traveltimes along six azimuths with increment 30° and obtained moveout velocities (dots in Figure 7a) by fitting a hyperbola to the exact moveout. Despite the complexity of the model, the best-fit ellipse found from the finite-spread moveout velocities (dashed) are sufficiently close to the theoretical NMO ellipse (solid) computed from equations (28) and (3). A small difference between the ellipses is caused by nonhyperbolic moveout associated with both anisotropy and vertical inhomogeneity. It is clear from Figure 7b that the influence of nonhyperbolic moveout becomes substantial only at source-receiver offsets that exceed the distance between the CMP and the reflector.

A similar example, but this time for a laterally inhomogeneous medium above the reflector is shown in Figure 8. The model contains three transversely isotropic layers with dipping lower boundaries and differently oriented symmetry axes. The NMO ellipse (solid) provides an excellent approximation to the effective moveout velocity (dots) for all four azimuths used in the computation, with a maximum error of just about 1.4%. In addition to verifying the accuracy of our algorithm based on the evaluation of the derivatives $\partial\mathbf{x}/\partial\gamma_n$ and $\partial\mathbf{p}/\partial\gamma_n$, this test demonstrates again that the analytic (zero-spread) normal-moveout velocity adequately describes P-wave

reflection traveltimes on conventional-length spreads.

FIELD-DATA EXAMPLE

The main purpose of the field-data example discussed here is to show how the generalized Dix formula can be applied to the extraction of interval NMO ellipses from reflection data. We used a 3-D P-wave data set acquired by ARCO (with funding from the Gas Research Institute) in the Powder River Basin, Wyoming, USA. A detailed description of this survey and preliminary processing results can be found in Corrigan et al. (1996) and Withers and Corrigan (1997). The goal of the experiment was to employ the azimuthal dependence of P-wave signatures in characterization of a fractured reservoir. Hence, the acquisition was carefully designed to provide a good offset coverage in a wide range of source-receiver azimuths. To enhance the signal-to-noise ratio, the data were collected into a number of "superbins," each with an almost random distribution of azimuths and offsets (Figure 9). Preprocessing included statics corrections and was designed to preserve the azimuthal dependence of reflection traveltimes (Corrigan et al. 1996; Withers and Corrigan 1997).

Figure 10 displays the composite CMP gather for one of the superbins in an azimuthal sector 20° wide (i.e., the sector includes all source-receiver traces with azimuths different by less than 20°); two prominent reflection events used in the analysis below are marked by arrows. According to Withers and Corrigan (1997), the reflection at a two-way vertical time of 2.14 s corresponds to the bottom of the Frontier/Niobrara formations, and the event at 2.58 s is the basement reflection. The traces are fairly noisy, which is typical for land acquisition, but the data quality was sufficient for azimuthal velocity analysis.

Below we show the results of our velocity analysis for a typical superbin from the survey area. One possible way to obtain the NMO ellipse for a given reflection is to divide the data into a number of azimuthal sectors (bins), determine the best-fit

stacking (moveout) velocity for each sector and approximate the angular stacking-velocity dependence with an elliptical function. We found, however, that the results of this analysis are often influenced by the number and size of the azimuthal sectors. A more stable way to reconstruct the NMO-velocity function is to perform semblance analysis for the whole superbin at each zero-offset time. Our approach is based on a 3-D semblance scan over the components of the matrix **W** [see equation (3)] using the hyperbolic moveout equation (1). (Since the maximum offset was a little smaller than the depth of the basement, the moveout for both events was close to hyperbolic.) To make this search less time consuming, we first obtain the best-fit "isotropic" (i.e., azimuth-independent) velocity $V_{\rm nmo}$ and then scan over two relatively small quantities responsible for the deviation of the NMO ellipse from the already obtained average "NMO circle." Application of efficient minimization algoritms makes the second stage relatively fast and allows us to avoid a full-scale 3-D scanning.

As illustrated by Figure 11, accounting for the azimuthal variation of stacking (moveout) velocity has no visible influence on the semblance peaks for the reflection at 2.14 s and a weaker event at about 2.32 s, which means that the NMO velocity for these reflections is practically independent of azimuth. In contrast, the azimuthal velocity analysis does increase the value of semblance for the deeper (basement) reflection by about 10%. Since for the two shallow events application of the elliptical NMO equation failed to produce any noticeable change in the semblance value, the 10% increase for the deepest event stands out enough to be diagnostic of a non-negligible (although, definitely, not large) azimuthal variation of stacking velocity. This example shows that mixing up all source-receiver azimuths in stacking-velocity analysis (as is conventionally done in 3-D processing) may impair the quality of stack in the presence of azimuthal anisotropy.

Thus, Figure 11 indicates that the azimuthal dependence of stacking velocity for this particular superbin is non-negligible only for the reflection at $t_0 = 2.58s$. This observation is confirmed by the shape of the effective NMO ellipses for both

events obtained from semblance analysis (Figure 12a). The stacking velocity of the basement reflection along the semi-major axis of the ellipse is almost 4% higher than in the orthogonal direction; the corresponding number for the reflection at 2.14 s is just 0.6%. Clearly, even for the basement event the azimuthal variation of NMO velocity in the study area is relatively weak, which complicates reliable reconstruction of NMO ellipses from reflection moveout. Note, however, that the generalized Dix equation applied here remains valid irrespective of how elongated the ellipses are.

Since the dips in the survey area are extremely small (Corrigan et al. 1996), the azimuthal dependence of stacking velocity can be attributed to the influence of azimuthal anisotropy associated with vertical fractures (the presence of fractures in this area was established by using borehole and shear-wave methods). To study the *interval* properties for vertical times between 2.14 and 2.58 s, we applied the generalized Dix equation (29) to the effective NMO ellipses. The pronounced azimuthal variation in the interval NMO velocity (12.3%, Figure 12b) can be explained by the intense fracturing in the layer immediately above the basement. The direction of the semi-major axis of the interval NMO ellipse is in general agreement with the predominant fracture orientation in the deeper part of the section determined from borehole data and shear-wave splitting analysis (Withers and Corrigan 1997). Complete processing/inversion results for the survey area will be reported in forthcoming publications.

DISCUSSION AND CONCLUSIONS

Azimuth-dependent normal-moveout velocity around a certain CMP location is described by a simple quadratic form and usually defines an *elliptical* curve if plotted in each azimuthal direction. The orientation and semi-axes of the ellipse are determined by the properties of the medium and the direction of the reflector normal at the zero-offset reflection point. Using this general result obtained by Grechka and

Tsvankin (1998), we have presented a series of solutions for the exact normal-moveout velocity of pure modes in anisotropic models of various complexity.

For a homogeneous anisotropic layer above a dipping reflector, NMO velocity was found explicitly as a function of the slowness vector corresponding to the zero-offset ray. This single-layer equation is valid for arbitrary anisotropic symmetry and any orientation of the CMP line. The vertical component of the slowness vector and its derivatives with respect to the horizontal slownesses, needed to compute the NMO velocity, can be obtained in an explicit form using the Christoffel equation. In addition to simplifying moveout modeling, our NMO equation can be effectively used in moveout inversion, as well as in developing weak-anisotropy approximations for different symmetries.

If the model contains a stack of homogeneous arbitrarily anisotropic layers above a dipping reflector, the NMO ellipse should be obtained by a Dix-type averaging of the single-layer expressions described above. Instead of the squared NMO velocities in the conventional Dix formula, our generalized equation operates with the interval matrices $\mathbf{W}_\ell$ that describe the NMO *ellipses* corresponding to the individual layers. To find azimuth-dependent normal-moveout velocity, it is sufficient to compute the zero-offset traveltime and the interval NMO ellipses for the slowness vector of the zero-offset ray. The generalized Dix equation can be used to perform moveout-based interval parameter estimation in vertically inhomogeneous anisotropic models of any symmetry. It should be emphasized, however, that application of the generalized Dix differentiation to dipping events entails full-scale layer-stripping because the corresponding NMO ellipses in the individual layers cannot be directly measured from the data.

One important special case considered in detail is a model with the same (through-going) vertical symmetry plane in all layers that also coincides with the dip plane of the reflector (e.g., the medium above the reflector is TI with a vertical symmetry axis). Because of the mirror symmetry with respect to the dip plane, the axes of

the NMO ellipse are aligned with the dip and strike directions of the reflector. The generalized Dix equation in such a model reduces to the rms averaging of the dip-line and strike-line NMO velocities in the individual layers (these averages determine the semi-axes of the NMO ellipse). This result represents a 3-D extension of the Dix-type equation developed by Alkhalifah and Tsvankin (1995) for normal moveout in the dip plane of the reflector.

Except for this special case, the effective NMO velocity computed by the Dix rms averaging generally takes an oval *anelliptic* form that thus deviates from the exact NMO ellipse. Still, this deviation is not significant if the interval NMO ellipses are close to being circles, which implies the absence of large dips and of significant azimuthal anisotropy. In any case, it is preferable to apply the generalized Dix equation (as opposed to the conventional Dix differentiation at a given azimuth) for *any* azimuthally anisotropic model because in addition to being more accurate it also provides the important advantage of smoothing the effective moveout velocities using the correct (elliptical) functional form and thus reducing the instability in interval parameter estimation. Application of the generalized Dix equation to moveout inversion in azimuthally anisotropic media using horizontal and dipping events is discussed in Grechka and Tsvankin (1997).

We complete the analysis by considering general inhomogeneous media and presenting an algorithm that leads to a significant reduction in the amount of computations needed to obtain the NMO velocity and conventional-spread reflection moveout. All information required to construct the NMO ellipse is contained in the results of the *dynamic* ray tracing (i.e., computation of geometrical spreading) of a single (zero-offset) ray. Although evaluation of geometrical spreading requires solving an additional system of differential equations together with the kinematic ray-tracing equations, this algorithm is orders of magnitude more efficient than multi-offset, multi-azimuth ray tracing. Furthermore, if the model consists of homogeneous layers or blocks separated by plane dipping interfaces, all quantities needed to find the NMO

ellipse can be computed during the kinematic tracing of the zero-offset ray.

The normal-moveout velocity discussed here is defined in the zero-spread limit and cannot account for nonhyperbolic moveout caused by anisotropy and inhomogeneity on finite-spread CMP gathers. Nevertheless, our numerical examples for various anisotropic models demonstrate that the hyperbolic moveout equation parameterized by NMO velocity provides good accuracy in the description of reflection moveout (especially that of P-waves) on conventional spreads close to the distance between the CMP and the reflector. Even if the hyperbolic moveout approximation becomes inadequate, NMO velocity can be obtained by means of nonhyperbolic moveout analysis (Tsvankin and Thomsen 1994; Sayers and Ebrom 1997). Hence, the results of this work can be efficiently used in traveltime inversion and dip-moveout processing for arbitrarily anisotropic media.

To show the feasibility of applying the generalized Dix equation in fracture detection, we processed wide-azimuth 3-D P-wave data acquired over a fractured reservoir in the Powder River Basin, Wyoming, USA. Azimuthal moveout analysis followed by the Dix differentiation allowed us to estimate the fracture orientation and magnitude of azimuthal anisotropy (measured by P-wave moveout velocity) in several intervals of interest. The direction of the semi-major axis of the interval NMO ellipse in the strongly anisotropic layer above the basement is in agreement with the known fracture trend in this part of the section.

ACKNOWLEDGMENTS

We are grateful to Dennis Corrigan and Robert Withers of ARCO for providing the field data and sharing their knowledge of the processing and interpretation issues. We would like to thank Bruce Mattocks and Bob Benson (both of CSM) for helping us in data processing and Ken Larner (CSM), Andreas Rüger (CSM; now at Landmark) and the referees of *Geophysical Prospecting* for their reviews of the paper.

The support for this work was provided by the members of the Consortium Project on Seismic Inverse Methods for Complex Structures at Center for Wave Phenomena, Colorado School of Mines and by the United States Department of Energy (project "Velocity Analysis, Parameter Estimation, and Constraints on Lithology for Transversely Isotropic Sediments" within the framework of the Advanced Computational Technology Initiative).

REFERENCES

Al-Dajani A. and Tsvankin I. 1996. Nonhyperbolic reflection moveout for horizontal transverse isotropy. 66th SEG Meeting, Denver, Expanded Abstracts, 1495–1498.

Alkhalifah T. 1997. Seismic data processing in vertically inhomogeneous TI media. *Geophysics* **62**, 662–675.

Alkhalifah T. and Tsvankin I. 1995. Velocity analysis in transversely isotropic media. *Geophysics* **60**, 1550–1566.

Červeny V. 1972. Seismic rays and ray intensities in inhomogeneous anisotropic media. *Geophysical Journal of the Royal Astronomical Society* **29**, 1–13.

Červeny V., Molotkov I.A. and Pšenčík I. 1977. *Ray method in seismology*. University of Karlova.

Cohen, J.K. 1998. A convenient expression for the NMO velocity function in terms of ray parameter. *Geophysics* **63**, 275–278.

Corrigan D., Withers R., Darnall J. and Skopinski T. 1996. Fracture mapping from azimuthal velocity analysis using 3D surface seismic data. 66th SEG Meeting, Denver, Expanded Abstracts, 1834–1837.

Dix C.H. 1955. Seismic velocities from surface measurements. *Geophysics* **20**, 68–86.

Gajewski D. and Pšenčík I. 1987. Computation of high-frequency seismic wavefields in 3-D laterally inhomogeneous anisotropic media. *Geophysical Journal of the Royal Astronomical Society* **91**, 383–411.

Gajewski D. and Pšenčík I. 1996. qP-wave phase velocities in weakly anisotropic media – perturbation approach. 66th SEG Meeting, Denver, Expanded Abstracts, 1507–1510.

Grechka V. and Tsvankin I. 1997. Moveout velocity analysis and parameter estiamtion for orthorhombic media. 67th SEG Meeting, Dallas, Expanded Abstracts, 1226–1229.

Grechka V. and Tsvankin I. 1998. 3-D description of normal moveout in anisotropic inhomogeneous media. *Geophysics* **63**, 1079–1092.

Hale D., Hill N. R. and Stefani J. 1992. Imaging salt with turning wave seismic waves. *Geophysics* **57**, 1453–1462.

Hubral P. and Krey T. 1980. *Interval velocities from seismic reflection measurements.* Society of Exploration Geophysicists.

Kashtan B.M. 1982. Calculation of geometrical spreading in piecewise homogeneous anisotropic media. *Problems of dynamic theory of seismic wave propagation* **22**, 14–24 (in Russian).

Kendall J-M. and Thomson C.J. 1989. A comment on the form of the geometrical spreading equations, with some examples of seismic ray tracing in inhomogeneous anisotropic media. *Geophysical Journal International* **99**, 401–413.

Levin F.K. 1971. Apparent velocity from dipping interface reflections. *Geophysics* **36**, 510–516.

Mensch T. and Rasolofosaon P. 1997. Elastic-wave velocities in anisotropic media of arbitrary symmetry – generalization of Thomsen's parameters ϵ, δ, and γ. *Geophysical Journal International* **128**, 43–64.

Sayers C.M. and Ebrom D.A. 1997. Seismic traveltime analysis for azimuthally anisotropic media: Theory and experiment. *Geophysics* **62**, 1570–1582.

Shah P.M. 1973. Use of wavefront curvature to relate seismic data with subsurface parameters. *Geophysics* **38**, 812–825.

Thomsen L. 1986. Weak elastic anisotropy. *Geophysics* **51**, 1954–1966.

Tsvankin I. 1995. Normal moveout from dipping reflectors in anisotropic media. *Geophysics* **60**, 268–284.

Tsvankin I. 1997a. Reflection moveout and parameter estimation for horizontal transverse isotropy. *Geophysics* **62**, 614–629.

Tsvankin I. 1997b. Anisotropic parameters and P-wave velocity for orthorhombic media. *Geophysics* **62**, 1292–1309.

Tsvankin I. and Thomsen L. 1994. Nonhyperbolic reflection moveout in anisotropic media. *Geophysics* **59**, 1290–1304.

Withers R. and Corrigan D. 1997. Fracture detection using wide azimuth 3D seismic surveys. 59th EAGE Conference, Geneva, Extended Abstracts, Paper E003.

APPENDIX A–RELATION BETWEEN THE MATRIX W AND THE NMO-VELOCITY ELLIPSE

Azimuth-dependent normal-moveout velocity is described by equation (3) of the main text as a general second-order curve in the horizontal plane. The expression for $V_{\rm nmo}(\alpha)$ can be simplified further by aligning the horizontal coordinate axes with the eigenvectors of the symmetric matrix $\mathbf{W}$ (Grechka and Tsvankin 1998). This rotation reduces equation (3) to

$$V_{\rm nmo}^{-2}(\alpha) = \lambda_1 \cos^2(\alpha - \beta) + \lambda_2 \sin^2(\alpha - \beta)\,, \tag{A-1}$$

where λ_1 and λ_2 are the eigenvalues of the matrix $\mathbf{W}$, and β is the angle between the eigenvector corresponding to λ_1 and the x_1-axis.

To verify the equivalence between equations (A-1) and (3), we expand

$$\cos^2(\alpha - \beta) = \cos^2\alpha \cos^2\beta + 2\sin\alpha \sin\beta \cos\alpha \cos\beta + \sin^2\alpha \sin^2\beta$$

and

$$\sin^2(\alpha - \beta) = \cos^2\alpha \sin^2\beta - 2\sin\alpha \sin\beta \cos\alpha \cos\beta + \sin^2\alpha \cos^2\beta\,.$$

Equations (A-1) and (3) are identical if

$$W_{11} = \lambda_1 \cos^2\beta + \lambda_2 \sin^2\beta\,, \tag{A-2}$$

$$W_{12} = \frac{1}{2}(\lambda_1 - \lambda_2)\,\sin 2\beta\,, \tag{A-3}$$

and

$$W_{22} = \lambda_1 \sin^2\beta + \lambda_2 \cos^2\beta\,. \tag{A-4}$$

Inverting equations (A-2) – (A-4) for $\lambda_{1,2}$ and β yields

$$\lambda_{1,2} = \frac{1}{2}\left[W_{11} + W_{22} \pm \sqrt{(W_{11} - W_{22})^2 + 4W_{12}^2}\right] \tag{A-5}$$

and

$$\tan\beta = \frac{W_{22} - W_{11} + \sqrt{(W_{22} - W_{11})^2 + 4W_{12}^2}}{2W_{12}}\,, \qquad (W_{12} \neq 0)\,. \tag{A-6}$$

Equations (A-5) and (A-6) show that $\lambda_{1,2}$ are indeed the eigenvalues of $\mathbf{W}$ and $\tan\beta$ is equal to the ratio of the components "2" and "1" of the eigenvector corresponding to λ_1. If $W_{12} = 0$, the matrix $\mathbf{W}$ is diagonal, and equation (3) reduces to equation (A-1) without any rotation.

As follows from equation (A-1), $V_{\rm nmo}(\alpha)$ represents an ellipse in the horizontal plane if the eigenvalues $\lambda_{1,2}$ are positive (Grechka and Tsvankin 1998). The "principal" values of the azimuth-dependent NMO velocity (the semi-axes of the ellipse) are given by

$$V_{\rm nmo}^{(i)} = \frac{1}{\sqrt{\lambda_i}}, \qquad (i = 1, 2)\,. \tag{A-7}$$

APPENDIX B–NMO VELOCITY IN A SINGLE LAYER

Here, we obtain the exact expression for the NMO velocity from a dipping reflector beneath a homogeneous arbitrarily anisotropic layer. The derivation is based on the general equations (3) and (4) describing the NMO ellipse and follows the approach suggested for the 2-D case by Cohen (1998).

To evaluate the derivatives $\partial x_i/\partial p_j$, we have to relate the horizontal ray displacements (x_1, x_2) between the zero-offset reflection point and the surface to the horizontal components of the slowness vector (p_1, p_2). We start by introducing the group-velocity vector $\mathbf{g}$,

$$x_i = g_i \tau \,, \qquad (i = 1, 2, 3) \,, \tag{B-1}$$

where τ is the one-way traveltime. Using the fact that the projection of the group-velocity vector on the slowness direction is equal to phase velocity, we can write

$$\mathbf{p} \cdot \mathbf{g} = p_1 g_1 + p_2 g_2 + p_3 g_3 = 1 \,. \tag{B-2}$$

Differentiating equation (B-2) with respect to p_i ($i = 1, 2$) and taking into account that the vertical slowness component p_3 can be considered as a function of p_1 and p_2 yields

$$g_i = -\frac{\partial p_3}{\partial p_i} g_3 - \mathbf{p} \cdot \frac{\partial \mathbf{g}}{\partial p_i} \,, \qquad (i = 1, 2) \,.$$

Since the slowness vector $\mathbf{p}$ is normal to the group-velocity surface (wavefront) $\mathbf{g}(p_1, p_2)$, while the vectors $\partial \mathbf{g}/\partial p_i$ are tangent to this surface, $\mathbf{p} \cdot \frac{\partial \mathbf{g}}{\partial p_i} = 0$. Hence,

$$g_i = -q_{,i} g_3 \,, \qquad (i = 1, 2) \,, \tag{B-3}$$

where $q \equiv q(p_1, p_2) \equiv p_3$ denotes the vertical slowness, and $q_{,i} \equiv \partial q/\partial p_i$. Substitution of equations (B-3) into equation (B-2) gives a representation of the vertical group-velocity component that will be needed later in the derivation:

$$g_3 = \frac{1}{q - p_1 q_{,1} - p_2 q_{,2}}. \tag{B-4}$$

Using equations (B-3), we rewrite the horizontal ray displacements x_i $(i = 1, 2)$ from equations (B-1) as

$$x_i = -q_{,i} g_3 \tau\,, \qquad (i = 1, 2)\,. \tag{B-5}$$

Note that $g_3\tau$ is the depth of the zero-offset reflection point, which is independent of the slowness components (p_1, p_2). Therefore, differentiating equations (B-5) yields

$$Y_{ij} \equiv \frac{\partial x_i}{\partial p_j} = -q_{,ij} g_3 \tau\,, \tag{B-6}$$

where $q_{,ij} \equiv \partial^2 q / \partial p_i \partial p_j$ is a symmetric matrix of the second derivatives of the vertical slowness.

The NMO ellipse is determined by the matrix $\mathbf{W}$ [equation (4)],

$$\mathbf{W} = \tau_0 \mathbf{Y}^{-1}\,, \tag{B-7}$$

where the inverse matrix $\mathbf{Y}^{-1}$ should be evaluated for the horizontal slowness components of the zero-offset ray.

Substituting Y_{ij} from equation (B-6) into equation (B-7) and using expression (B-4) for g_3, we obtain

$$\mathbf{W} = \tau_0 \mathbf{Y}^{-1} = \frac{p_1 q_{,1} + p_2 q_{,2} - q}{q_{,11} q_{,22} - q_{,12}^2} \begin{pmatrix} q_{,22} & -q_{,12} \\ -q_{,12} & q_{,11} \end{pmatrix}. \tag{B-8}$$

With the matrix $\mathbf{W}$ from equation (B-8), equation (3) of the NMO ellipse in a homogeneous arbitrarily anisotropic layer takes the following form:

$$\begin{aligned} V_{\rm nmo}^{-2}(\alpha) &\equiv V_{\rm nmo}^{-2}(\alpha, p_1, p_2) \\ &= \frac{p_1 q_{,1} + p_2 q_{,2} - q}{q_{,11} q_{,22} - q_{,12}^2} \left[q_{,22} \cos^2\alpha - 2 q_{,12} \sin\alpha \cos\alpha + q_{,11} \sin^2\alpha \right]. \end{aligned} \tag{B-9}$$

APPENDIX C–RELATION BETWEEN THE EXACT AND RMS-AVERAGED NMO VELOCITY

Here, we examine the accuracy of the rms averaging of the interval NMO velocities for a model that consists of a stack of horizontal arbitrarily anisotropic layers above a dipping reflector. The interval NMO velocity in the ℓ-th layer is given by equation (3):

$$V_{\mathrm{nmo},\ell}^{-2}(\alpha) = W_{11,\ell}\cos^2\alpha + 2\,W_{12,\ell}\sin\alpha\cos\alpha + W_{22,\ell}\sin^2\alpha\,. \tag{C-1}$$

The symmetric matrix $\mathbf{W}_\ell$ is expressed through its eigenvalues $\lambda_{1,\ell}$ and $\lambda_{2,\ell}$ in equations (A-2) – (A-4). Here, we assume that $\lambda_{1,\ell} > \lambda_{2,\ell}$:

$$\lambda_{2,\ell} \equiv \lambda_\ell\,,$$

$$\lambda_{1,\ell} \equiv \lambda_\ell(1+\mu_\ell)\,, \tag{C-2}$$

where

$$\mu_\ell > 0\,,$$

for all ℓ.

An approximate NMO velocity is obtained by rms averaging of the interval values at the azimuth α [equation (C-1)] as

$$\tilde{V}_{\mathrm{nmo}}^2(L,\alpha) = \frac{1}{\tau(L)}\sum_{\ell=1}^{L}\tau_\ell\,\Big[W_{11,\ell}\cos^2\alpha + 2\,W_{12,\ell}\sin\alpha\cos\alpha + W_{22,\ell}\sin^2\alpha\Big]^{-1} \tag{C-3}$$

In general, $\tilde{V}_{\mathrm{nmo}}(L,\alpha)$ from equation (C-3) may be thought of as an approximation of the exact normal-moveout velocity $V_{\mathrm{nmo}}(L,\alpha)$ from equation (3),

$$\begin{aligned} V_{\mathrm{nmo}}^2(L,\alpha) &= \Big[\,W_{11}(L)\cos^2\alpha + 2\,W_{12}(L)\sin\alpha\cos\alpha + W_{22}(L)\sin^2\alpha\,\Big]^{-1} \\ &= \Big[\,W_{11}^{-1}(L)W_{22}^{-1}(L) - (W_{12}^{-1}(L))^2\,\Big] \\ &\quad\times\Big[\,W_{22}^{-1}(L)\cos^2\alpha - 2\,W_{12}^{-1}(L)\sin\alpha\cos\alpha + W_{11}^{-1}(L)\sin^2\alpha\,\Big]^{-1}\,, \end{aligned} \tag{C-4}$$

where $W_{ij}^{-1}(L)$ are the elements of the inverse matrix $\mathbf{W}^{-1}(L)$ given by the Dix-type equation (28):

$$\mathbf{W}^{-1}(L) = \frac{1}{\tau(L)} \sum_{\ell=1}^{L} \tau_\ell \, \mathbf{W}_\ell^{-1} \, . \tag{C-5}$$

Clearly, the direct rms averaging of NMO velocities in equation (C-3) is different from the more complicated averaging of the inverse matrices $\mathbf{W}_\ell^{-1}$ [equation (C-5)] used to obtain the exact NMO velocity in equation (C-4). Nevertheless, we will show that the two representations of the NMO velocity become identical in the *linear* approximation with respect to μ_ℓ, i.e.,

$$\tilde{V}_{\rm nmo}(L,\alpha) = V_{\rm nmo}(L,\alpha) + O(\mu_\ell^2) \, . \tag{C-6}$$

In the following derivation, we keep only terms independent of or linear in μ_ℓ. Combining equations (C-2) and (A-2) – (A-4) allows us to express the interval matrices $\mathbf{W}_\ell$ through the eigenvalue λ_ℓ and μ_ℓ,

$$\begin{aligned} W_{11,\ell} &= \lambda_\ell \, (1 + \mu_\ell \cos^2 \beta_\ell) \, , \\ W_{12,\ell} &= \lambda_\ell \, \mu_\ell \sin \beta_\ell \cos \beta_\ell \, , \\ W_{22,\ell} &= \lambda_\ell \, (1 + \mu_\ell \sin^2 \beta_\ell) \, , \end{aligned} \tag{C-7}$$

where β_ℓ are the rotation angles of the interval NMO ellipses introduced in Appendix A.

Substituting equation (C-7) into equation (C-3), we find the following linearized (in μ_ℓ) expression for the rms-averaged NMO velocity:

$$\tilde{V}_{\rm nmo}^2(L,\alpha) = \frac{1}{\tau(L)} \sum_{\ell=1}^{L} \frac{\tau_\ell}{\lambda_\ell} \left[1 - \mu_\ell \cos^2(\alpha - \beta_\ell) \right] \, . \tag{C-8}$$

Next, we need to evaluate the effective NMO ellipse [equation (C-4)] in the same approximation. Using equation (C-7) and dropping terms quadratic in μ_ℓ, we represent the inverse matrices $\mathbf{W}_\ell^{-1}$ as

$$\mathbf{W}_\ell^{-1} = \frac{1}{\lambda_\ell} \begin{pmatrix} 1 - \mu_\ell \cos^2 \beta_\ell & -\mu_\ell \sin \beta_\ell \cos \beta_\ell \\ -\mu_\ell \sin \beta_\ell \cos \beta_\ell & 1 - \mu_\ell \sin^2 \beta_\ell \end{pmatrix} . \tag{C-9}$$

After averaging the matrices (C-9) in accordance with equation (C-5) and substituting the result into equation (C-4), we obtain

$$V_{\rm nmo}^2(L, \alpha) = \frac{1}{\tau(L)} \sum_{\ell=1}^{L} \frac{\tau_\ell}{\lambda_\ell} \left[1 - \mu_\ell \cos^2(\alpha - \beta_\ell)\right] . \tag{C-10}$$

Since equations (C-8) and (C-10) are identical, the rms-averaged velocity $\tilde{V}_{\rm nmo}$ is indeed equal to the exact NMO velocity in the linear approximation with respect to μ_ℓ [equation (C-6)]. Therefore, $\tilde{V}_{\rm nmo}$ should represent a good approximation in models with small and *moderate* values of μ_ℓ, for which terms quadratic in μ_ℓ can be ignored.

FIGURES

FIG. 1. Normal-moveout velocity is calculated on CMP lines with different azimuths and a fixed midpoint location.

FIG. 2. Comparison of the P-wave NMO velocity from equation (8) (solid line) and the moveout (stacking) velocity (dots) obtained by least-squares fitting of a hyperbola to the exact traveltimes computed for speadlength equal to the distance between the CMP and the reflector. The model contains a homogeneous orthorhombic layer (with the vertical symmetry planes at azimuths 0° and 90°) above a plane dipping reflector; the dip and azimuth of the reflector are equal to 30° (azimuthal angles are shown along the perimeter of the plot). The relevant medium parameters [in Tsvankin's (1997b) notation] are $V_{P0} = 2.0$ km/s, $\epsilon^{(1)} = 0.110$, $\delta^{(1)} = -0.035$, $\epsilon^{(2)} = 0.225$, $\delta^{(2)} = 0.100$, $\delta^{(3)} = 0$. The vertical symmetry plane at zero azimuth has the properties of the VTI model of Dog Creek shale, while the second vertical symmetry plane is equivalent to Taylor sandstone; both models are described in Thomsen (1986).

FIG. 3. A dipping reflector beneath a horizontally layered overburden. Normal-moveout velocity in this model can be obtained from the generalized Dix equation derived here.

FIG. 4. Comparison of the exact P-wave NMO ellipse (solid line) and an approximate NMO velocity obtained by the Dix-type averaging [equation (C-3), dashed line]. The model contains three horizontal orthorhombic layers with a horizontal ($[x_1, x_2]$) symmetry plane. The azimuth of the $[x_1, x_3]$ symmetry plane (also, the direction of one of the axes of the interval NMO ellipse) in the first (subsurface) layer is $\beta_1 = 0^\circ$, in the second layer – $\beta_2 = 45^\circ$, and in the third layer – $\beta_3 = 60^\circ$. The vertical P-wave velocities are $V_{P0,1} = 2.0$ km/s, $V_{P0,2} = 3.0$ km/s, and $V_{P0,3} = 3.5$ km/s; the interval zero-offset traveltimes are equal to each other ($\tau_1 = \tau_2 = \tau_3 = 1.0$ s).

The relevant anisotropic parameters [in Tsvankin's (1997b) notation] are (subscripts denote the layer number): Layer 1 – $\delta_1^{(1)} = 0.25$, $\delta_1^{(2)} = -0.15$, Layer 2 – $\delta_2^{(1)} = -0.20$, $\delta_2^{(2)} = 0.20$, Layer 3 – $\delta_3^{(1)} = 0.25$, and $\delta_3^{(2)} = -0.15$.

FIG. 5. The rms-averaged NMO velocity $\tilde{V}_{\rm nmo}$ [equation (C-3)] normalized by the exact value in *isotropic* media; the azimuth is measured with respect to the dip plane of the reflector. The model contains three layers above the reflector with the interval velocities $V_1 = 2.0$ km/s, $V_2 = 3.0$ km/s, and $V_2 = 3.5$ km/s and the interval zero-offset traveltimes $\tau_1 = \tau_2 = \tau_3 = 1.0$ s. The reflector dips are $\phi = 40^\circ$ (dotted line), $\phi = 60^\circ$ (dashed-dotted), $\phi = 70^\circ$ (dashed), and $\phi = 80^\circ$ (solid).

FIG. 6. The model used in Figure 7 to check the accuracy of the generalized Dix equation. Layer 1 is transversely isotropic with a vertical symmetry axis (VTI) and relevant parameters $V_{P0,1} = 2.5$ km/s, $\epsilon_1 = 0.2$, $\delta_1 = 0.1$. Layer 2 is TI with a horizontal symmetry axis (azimuth $\beta_2 = 30^\circ$) and $V_{P0,2} = 3.0$ km/s, $\epsilon_2^{(\rm V)} = -0.2$, $\delta_2^{(\rm V)} = -0.15$ (for HTI notation, see Tsvankin 1997a). Layer 3 is orthorhombic with $V_{P0,3} = 3.5$ km/s, $\epsilon_3^{(1)} = 0.2$, $\delta_3^{(1)} = 0.15$, $\epsilon_3^{(2)} = -0.3$, $\delta_3^{(2)} = -0.2$, $\delta_3^{(3)} = 0.05$; the azimuth of the $[x_1, x_3]$ symmetry plane $\beta_3 = 60^\circ$. The interface depths are $z_1 = 1.0$ km, $z_2 = 2.0$ km, $z_3 = 3.0$ km. The reflector dip is 20°, the azimuth of the dip plane is 0°.

FIG. 7. (a) Comparison between the theoretical P-wave NMO ellipse calculated from the generalized Dix equation (solid) and moveout velocities obtained from ray-traced traveltimes for spreadlength equal to the distance between the CMP and the reflector (dots). The model is shown in Figure 6; the dashed line marks the best-fit ellipse found from the finite-spread moveout velocities. (b) Hyperbolic moveout curve parameterized by the exact NMO velocity (solid) vs. computed traveltimes (dots) at azimuths 60° and 150°; D is the CMP-reflector distance.

FIG. 8. Comparison of the theoretical P-wave NMO ellipse (solid) and finite-spread moveout velocity (dots; the spreadlength is equal to the CMP-reflector distance) in an azimuthally-anisotropic model with dipping layers. The NMO ellipse is computed from equations (3) and (4), with the spatial derivatives of the ray parameter evaluated using equation (38). The model consists of three dipping transversely layers with different orientation of the symmetry axis. The first layer is VTI with $V_{P0,1} = 2.0$ km/s, $\epsilon_1 = 0.2$, and $\delta_1 = 0.1$. The second layer is HTI with the azimuth of the symmetry axis of 30° and $V_{P0,2} = 2.4$ km/s, $\epsilon_2 = 0.15$, $\delta_2 = 0$. The third layer is TI with a tilted symmetry axis (the azimuth is 60°, the tilt is 30°) and $V_{P0,3} = 3$ km/s, $\epsilon_3 = 0.25$, $\delta_3 = 0.08$ [for all layers we used the generic Thomsen's (1986) parameters]. The azimuth ψ and dip ϕ of the bottom of the first layer are $\psi_1 = 70°$ and $\phi_1 = 10°$; for the bottom of the second layer $\psi_2 = 20°$ and $\phi_2 = 15°$; for the reflector $\psi_3 = 50°$ and $\phi_3 = 35°$. The distances between the CMP and the interfaces are 1 km, 2 km, and 3 km.

FIG. 9. Plan view of the sourse and receiver positions for a typical superbin with a radius of 2 km. The maximum source-receiver offset is close to the depth of the basement; the basement reflection is recorded at about 2.58 s (see Figure 10).

FIG. 10. Common-midpoint gather composed of traces with source-receiver azimuths within a 20° azimuthal sector centered at N30E. Arrows mark the reflection events used in our analysis.

FIG. 11. Semblance curves obtained by conventional velocity analysis that ignores the azimuthal dependence of stacking velocity (dashed) and by our azimuthal velocity analysis (solid).

FIG. 12. (a) The effective NMO ellipses for the reflection events at 2.14 s (dashed) and 2.58 s (solid) reconstructed from the data. N4E is the azimuth of the semi-major axis of the NMO ellipse for the deeper event. (b) The corresponding interval NMO ellipse computed from the generalized Dix equation; the azimuth of the semi-major axis is N2E.

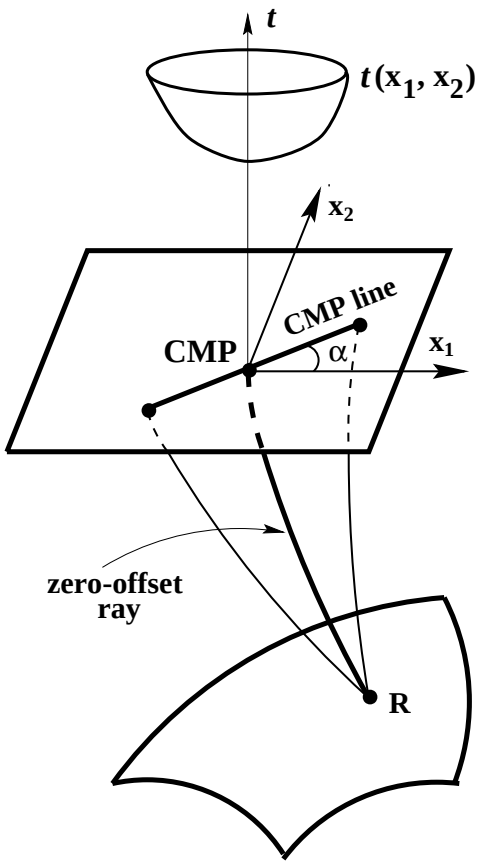

FIG. 1. Normal-moveout velocity is calculated on CMP lines with different azimuths and a fixed midpoint location.

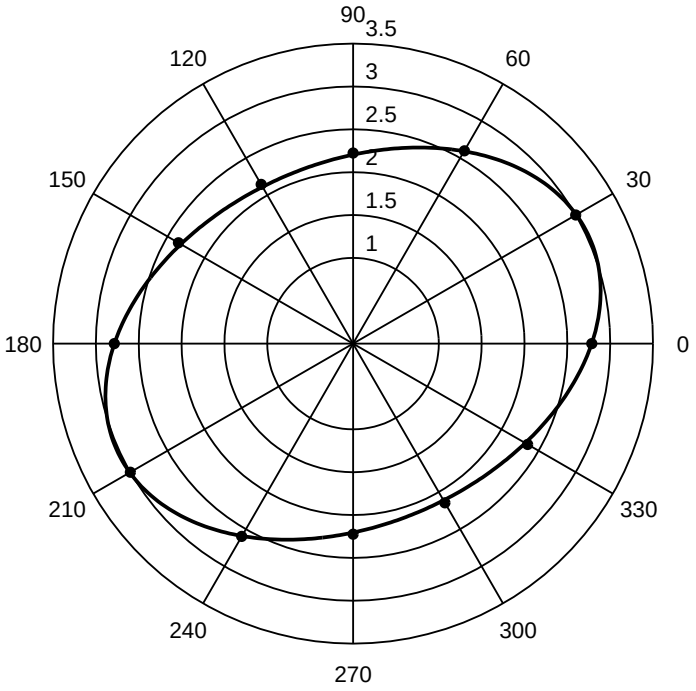

FIG. 2. Comparison of the P-wave NMO velocity from equation (8) (solid line) and the moveout (stacking) velocity (dots) obtained by least-squares fitting of a hyperbola to the exact traveltimes computed for speadlength equal to the distance between the CMP and the reflector. The model contains a homogeneous orthorhombic layer (with the vertical symmetry planes at azimuths 0° and 90°) above a plane dipping reflector; the dip and azimuth of the reflector are equal to 30° (azimuthal angles are shown along the perimeter of the plot). The relevant medium parameters [in Tsvankin's (1997b) notation] are $V_{P0} = 2.0$ km/s, $\epsilon^{(1)} = 0.110$, $\delta^{(1)} = -0.035$, $\epsilon^{(2)} = 0.225$, $\delta^{(2)} = 0.100$, $\delta^{(3)} = 0$. The vertical symmetry plane at zero azimuth has the properties of the VTI model of Dog Creek shale, while the second vertical symmetry plane is equivalent to Taylor sandstone; both models are described in Thomsen (1986).

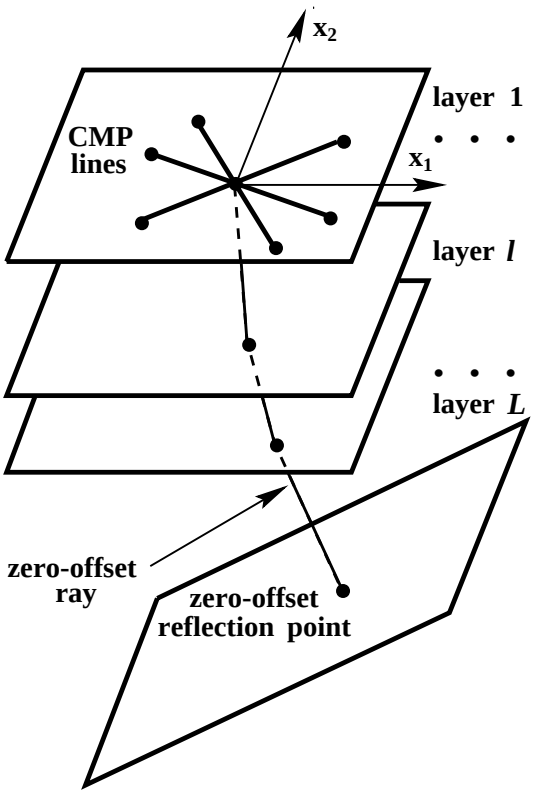

FIG. 3. A dipping reflector beneath a horizontally layered overburden. Normal-moveout velocity in this model can be obtained from the generalized Dix equation derived here.

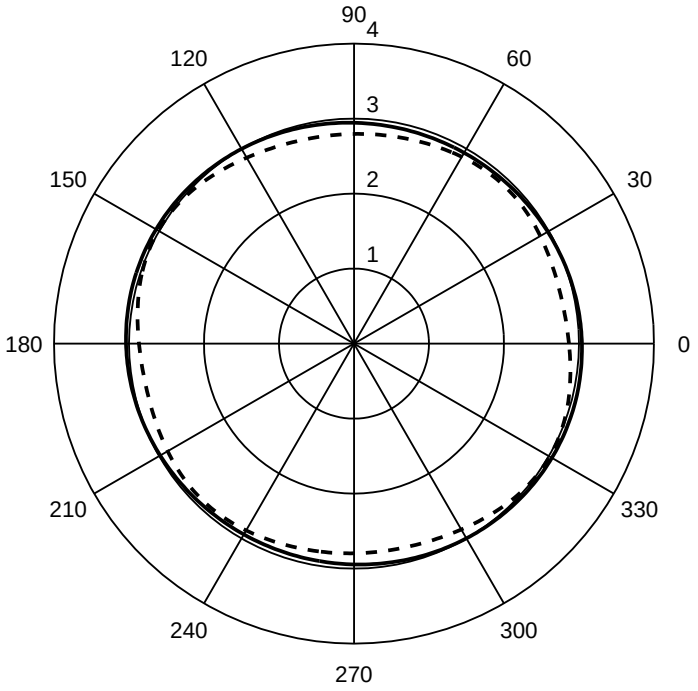

FIG. 4. Comparison of the exact P-wave NMO ellipse (solid line) and an approximate NMO velocity obtained by the Dix-type averaging [equation (C-3), dashed line]. The model contains three horizontal orthorhombic layers with a horizontal ($[x_1, x_2]$) symmetry plane. The azimuth of the $[x_1, x_3]$ symmetry plane (also, the direction of one of the axes of the interval NMO ellipse) in the first (subsurface) layer is $\beta_1 = 0^\circ$, in the second layer – $\beta_2 = 45^\circ$, and in the third layer – $\beta_3 = 60^\circ$. The vertical P-wave velocities are $V_{P0,1} = 2.0$ km/s, $V_{P0,2} = 3.0$ km/s, and $V_{P0,3} = 3.5$ km/s; the interval zero-offset traveltimes are equal to each other ($\tau_1 = \tau_2 = \tau_3 = 1.0$ s). The relevant anisotropic parameters [in Tsvankin's (1997b) notation] are (subscripts denote the layer number): Layer 1 – $\delta_1^{(1)} = 0.25$, $\delta_1^{(2)} = -0.15$, Layer 2 – $\delta_2^{(1)} = -0.20$, $\delta_2^{(2)} = 0.20$, Layer 3 – $\delta_3^{(1)} = 0.25$, and $\delta_3^{(2)} = -0.15$.

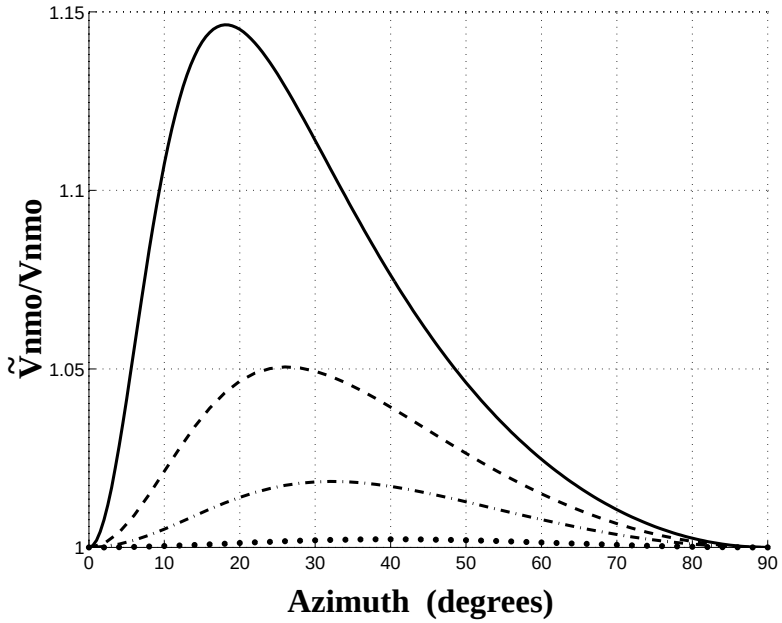

FIG. 5. The rms-averaged NMO velocity $\tilde{V}_{\rm nmo}$ [equation (C-3)] normalized by the exact value in *isotropic* media; the azimuth is measured with respect to the dip plane of the reflector. The model contains three layers above the reflector with the interval velocities $V_1 = 2.0$ km/s, $V_2 = 3.0$ km/s, and $V_2 = 3.5$ km/s and the interval zero-offset traveltimes $\tau_1 = \tau_2 = \tau_3 = 1.0$ s. The reflector dips are $\phi = 40^\circ$ (dotted line), $\phi = 60^\circ$ (dashed-dotted), $\phi = 70^\circ$ (dashed), and $\phi = 80^\circ$ (solid).

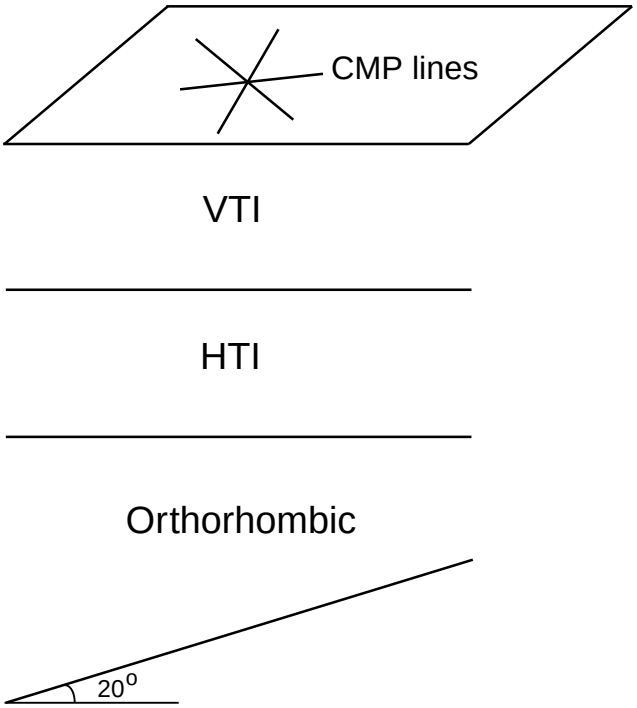

FIG. 6. The model used in Figure 7 to check the accuracy of the generalized Dix equation. Layer 1 is transversely isotropic with a vertical symmetry axis (VTI) and relevant parameters $V_{P0,1} = 2.5$ km/s, $\epsilon_1 = 0.2$, $\delta_1 = 0.1$. Layer 2 is TI with a horizontal symmetry axis (azimuth $\beta_2 = 30°$) and $V_{P0,2} = 3.0$ km/s, $\epsilon_2^{(\mathrm{V})} = -0.2$, $\delta_2^{(\mathrm{V})} = -0.15$ (for HTI notation, see Tsvankin 1997a). Layer 3 is orthorhombic with $V_{P0,3} = 3.5$ km/s, $\epsilon_3^{(1)} = 0.2$, $\delta_3^{(1)} = 0.15$, $\epsilon_3^{(2)} = -0.3$, $\delta_3^{(2)} = -0.2$, $\delta_3^{(3)} = 0.05$; the azimuth of the $[x_1, x_3]$ symmetry plane $\beta_3 = 60°$. The interface depths are $z_1 = 1.0$ km, $z_2 = 2.0$ km, $z_3 = 3.0$ km. The reflector dip is $20°$, the azimuth of the dip plane is $0°$.

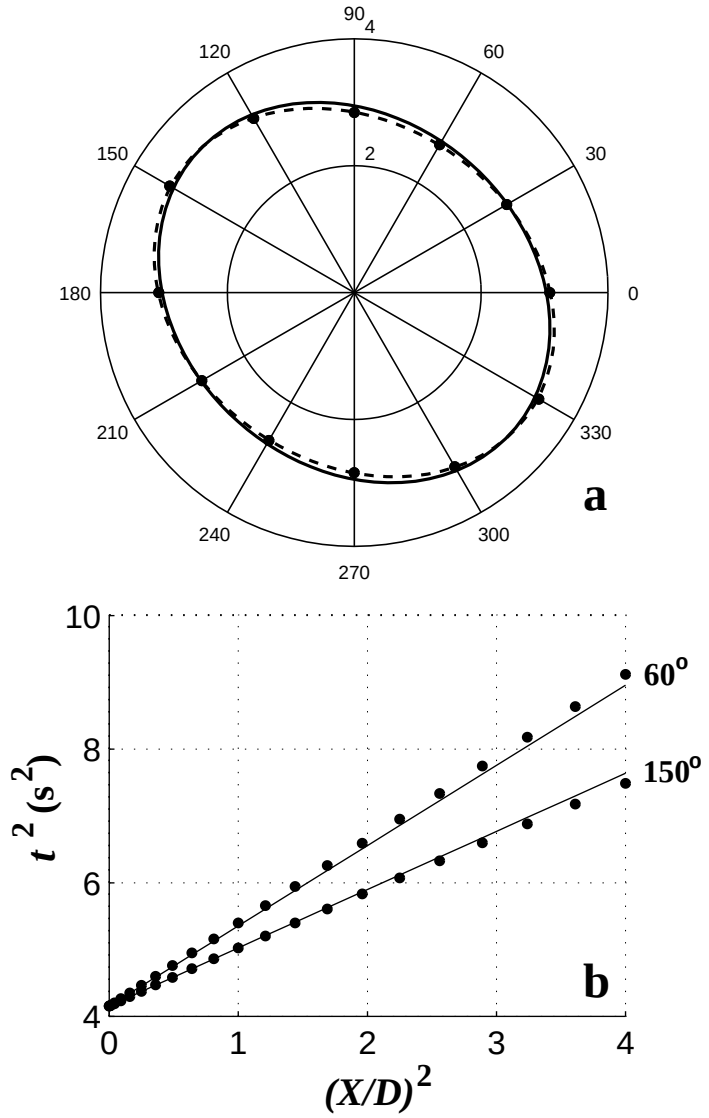

FIG. 7. (a) Comparison between the theoretical P-wave NMO ellipse calculated from the generalized Dix equation (solid) and moveout velocities obtained from ray-traced traveltimes for spreadlength equal to the distance between the CMP and the reflector (dots). The model is shown in Figure 6; the dashed line marks the best-fit ellipse found from the finite-spread moveout velocities. (b) Hyperbolic moveout curve parameterized by the exact NMO velocity (solid) vs. computed traveltimes (dots) at azimuths 60° and 150°; D is the CMP-reflector distance.

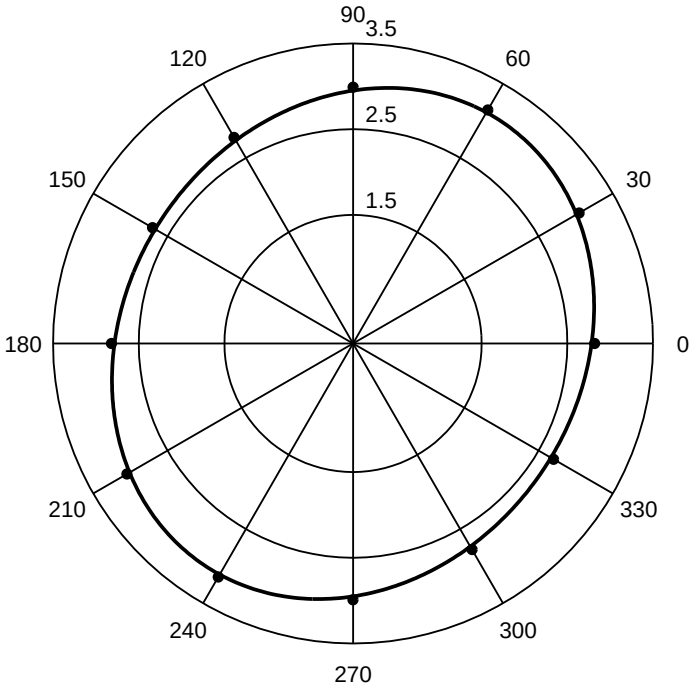

FIG. 8. Comparison of the theoretical P-wave NMO ellipse (solid) and finite-spread moveout velocity (dots; the spreadlength is equal to the CMP-reflector distance) in an azimuthally-anisotropic model with dipping layers. The NMO ellipse is computed from equations (3) and (4), with the spatial derivatives of the ray parameter evaluated using equation (38). The model consists of three dipping transversely layers with different orientation of the symmetry axis. The first layer is VTI with $V_{P0,1} = 2.0$ km/s, $\epsilon_1 = 0.2$, and $\delta_1 = 0.1$. The second layer is HTI with the azimuth of the symmetry axis of 30° and $V_{P0,2} = 2.4$ km/s, $\epsilon_2 = 0.15$, $\delta_2 = 0$. The third layer is TI with a tilted symmetry axis (the azimuth is 60°, the tilt is 30°) and $V_{P0,3} = 3$ km/s, $\epsilon_3 = 0.25$, $\delta_3 = 0.08$ [for all layers we used the generic Thomsen's (1986) parameters]. The azimuth ψ and dip ϕ of the bottom of the first layer are $\psi_1 = 70^\circ$ and $\phi_1 = 10^\circ$; for the bottom of the second layer $\psi_2 = 20^\circ$ and $\phi_2 = 15^\circ$; for the reflector $\psi_3 = 50^\circ$ and $\phi_3 = 35^\circ$. The distances between the CMP and the interfaces are 1 km, 2 km, and 3 km.

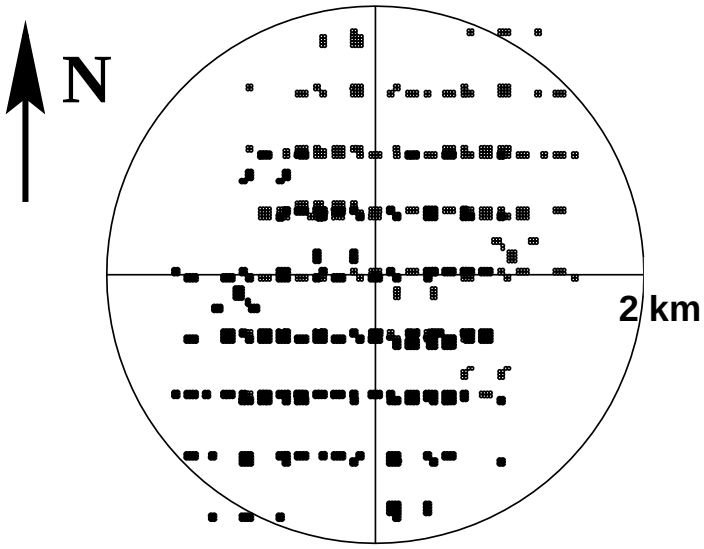

FIG. 9. Plan view of the sourse and receiver positions for a typical superbin with a radius of 2 km. The maximum source-receiver offset is close to the depth of the basement; the basement reflection is recorded at about 2.58 s (see Figure 10).

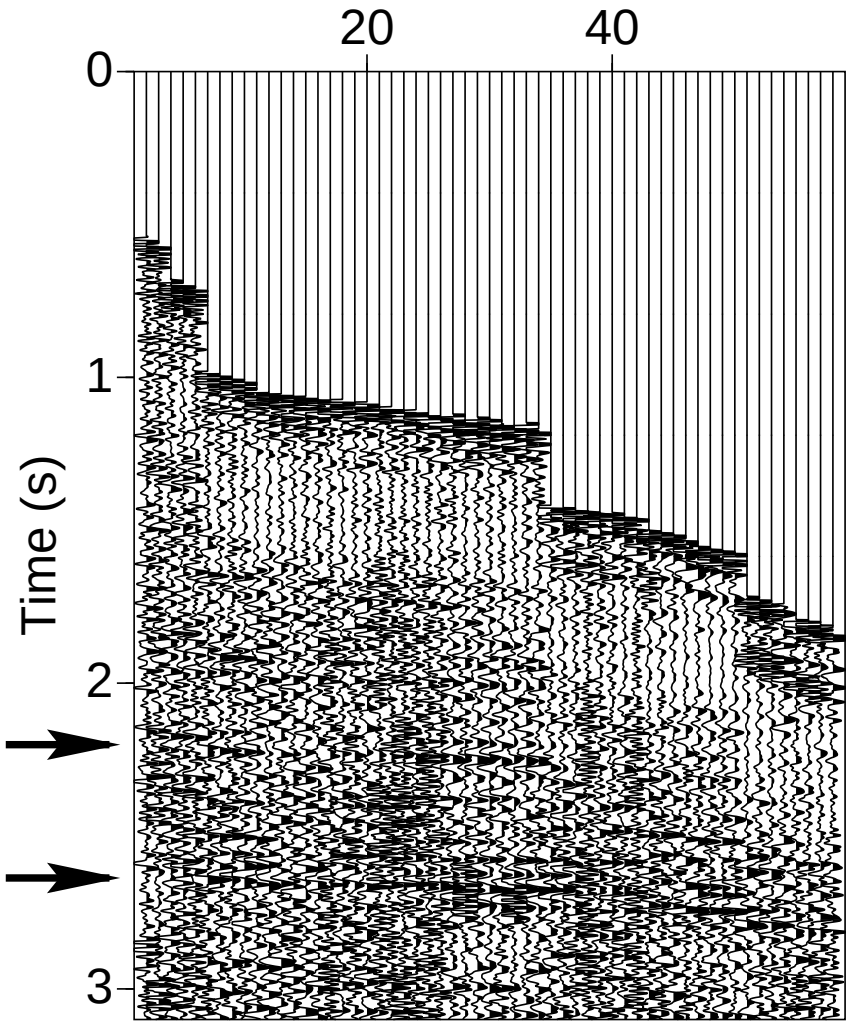

FIG. 10. Common-midpoint gather composed of traces with source-receiver azimuths within a 20° azimuthal sector centered at N30E. Arrows mark the reflection events used in our analysis.

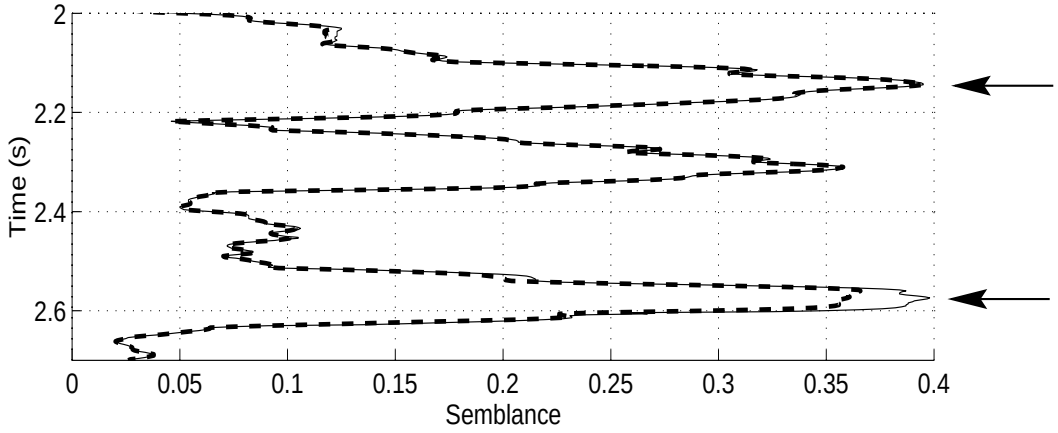

FIG. 11. Semblance curves obtained by conventional velocity analysis that ignores the azimuthal dependence of stacking velocity (dashed) and by our azimuthal velocity analysis (solid).

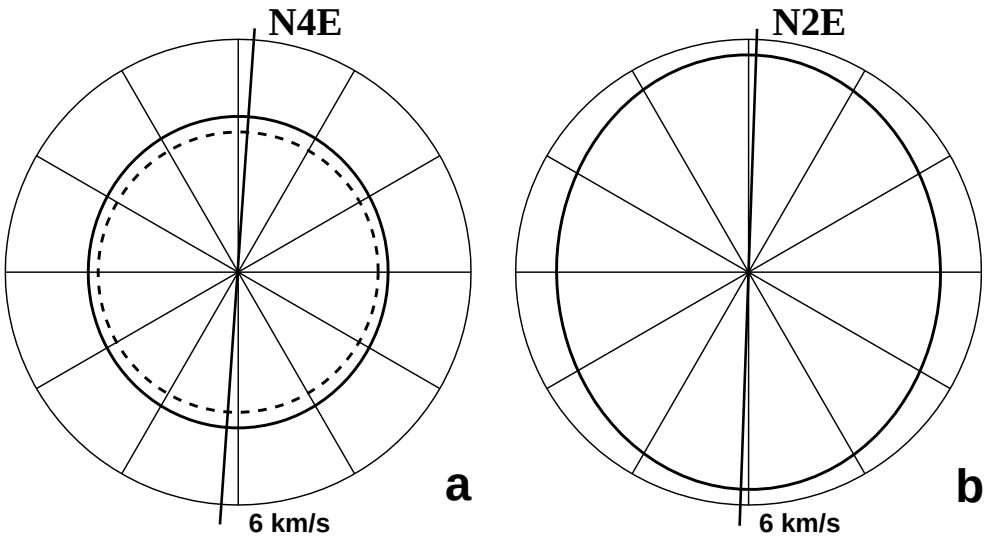

FIG. 12. (a) The effective NMO ellipses for the reflection events at 2.14 s (dashed) and 2.58 s (solid) reconstructed from the data. N4E is the azimuth of the semi-major axis of the NMO ellipse for the deeper event. (b) The corresponding interval NMO ellipse computed from the generalized Dix equation; the azimuth of the semi-major axis is N2E.